STRATIFICATION INFLUENCES ON INSTREAM CARBON CHEMISTRY AND EXPORT WITHIN A BEADED ARCTIC STREAM AND EVALUATION OF FLUORESCENCE INSTRUMENTATION

Katherine Hope Harrold

A thesis submitted to the faculty of the University of North Carolina at Chapel Hill in partial fulfillment of the requirements for the degree of Master of Science in the Department of Environmental Sciences and Engineering.

Chapel Hill
2013

Approved by:

Rose M. Cory

Stephen C. Whalen

George W. Kling

ABSTRACT

KATHERINE H. HARROLD: Stratification Influences on Instream Carbon Chemistry and Export within a Beaded Arctic Stream and Evaluation of Fluorescence Instrumentation
(Under the direction of Rose M. Cory)

I investigated the effect of stratification in beaded stream pools on the quantity and quality of dissolved organic matter (DOM). Soil waters feeding the pool bottom waters overlapped in chromophoric (CDOM) and fluorescent (FDOM) quantity and quality, while pool surface waters had on average 56 and 32 % less CDOM and FDOM, respectively, compared to pool bottom waters. The observed differences between pool surface and bottom waters were consistent with shifts in CDOM and FDOM following experimental photodegradation of pool bottom waters. To improve FDOM characterization across time and instruments, FDOM analysis was evaluated using the Aqualog, a new instrument optimized for FDOM, and the Fluoromax-4, a conventional spectrofluorometer, across a range of CDOM and FDOM concentrations. While the application of an empirical inter-instrument correction factor improved the inter-instrument FDOM comparison, inter-instrument variability was not fully removed by application of a range of correction factors.

ACKNOWLEDGEMENTS

I thank Dustin Carroll, Jason Dobkowski, Kellie Donajkowski, Sara Fortin, Jen Kostrewski, Amy Markstein, Oscar Marquina, Jamie Olson, Brittany Papworth, and Collin Ward for their assistance in sample collection and analysis of Imnavait Creek samples. Jason Stuckey created the bathymetric maps of the Imnavait Creek pools. I thank Yvonne Nguyen for her assistance in the analysis of many of the samples used to evaluate the Aqualog. Final publication submission of chapter one of my thesis will include Bethany T. Neilson, George W. Kling, Brittany N. Papworth, and Rose M. Cory as co-authors. Final publication submission of chapter two of my thesis will include Rose M. Cory as a co-author.

TABLE OF CONTENTS

LIST OF TABLES

Table

LIST OF FIGURES

Figure

LIST OF ABREVIATIONS AND SYMBOLS

$a_{CDOM,\lambda}$	Naperian absorption coefficient of CDOM at wavelength λ
A_{em}	Decadic absorbance by CDOM at the emission wavelength
A_{ex}	Decadic absorbance by CDOM at the excitation wavelength
A_{λ}	Absorbance reading at wavelength λ
C	Carbon
CCD	Charge-coupled device
CDOM	Chromophoric dissolved organic matter
CO_2	Carbon dioxide
$dec_{CDOM,254}$	decadic absorption coefficient of CDOM at 254 nm
DFB	Deferoxamine mesylate
DI	Laboratory grade deionized water
DOC	Dissolved organic carbon
DOM	Dissolved organic matter
EEM	Excitation-emission matrix
$emcorr_{FM\text{-}OrigHoriba}$	Original Horiba-provided emission correction factor for the Fluoromax-4
$emcorr_{FM\text{-}SRM}$	Emission correction factor generated using Horiba's NIST standard reference materials for the Fluoromax-4
$excorr_{FM\text{-}rhod}$	User-generated rhodamine excitation correction factor for the Fluoromax-4
$excorr_{FM\text{-}HoribaKit}$	Excitation correction factor created with a Horiba excitation correction kit (Excitation Correction Factor Kit, F-3028, Horiba) for the Fluoromax-4
ex/em	Excitation and emission wavelength pair

E_λ	Downwelling irradiance
FDOM	Fluorescent dissolved organic matter
FI	Fluorescence index
HCl	Hydrochloric acid
IFE	Inner-filter effect
$K_{d,\lambda}$	Attenuation coefficient at wavelength λ
l	pathlength
NIST	National Institute of Standards and Technology
PAR	Photosynthetically active radiation
Pg	Petagram
PLFA	Pony Lake fulvic acid
RU	Raman units
SE	Standard error
SD	Standard deviation
S_R	Slope ratio
SRFA	Suwannee River fulvic acid
$SUVA_{254}$	Specific UV absorbance at 254 nm
TMG	Trace-metal grade
z	Depth
$z_{1\%}$	Depth of 1% surface irradiance
λ	Wavelength

CHAPTER ONE

Stratification Influences on Instream Carbon Chemistry and Export within a Beaded Arctic Stream

I investigated the effect of stratification in pools of a beaded stream on the quantity and quality of dissolved organic matter (DOM) exported from Imnavait Creek in the Alaskan Arctic. Conductivity, pH, temperature, and dissolved oxygen measurements were used to evaluated stratification of the pools and further characterize the different waters. Analysis of the chromophoric (CDOM) and fluorescent (FDOM) fractions of the DOM pool were used to characterize the DOM in the soil water feeding into the pools, and the surface and bottom waters of the creek pools. Soil waters and pool bottom waters overlapped in CDOM and FDOM quantity and quality, while pool surface waters had on average 56 and 32 % less CDOM and FDOM, respectively, compared to pool bottom waters. There were also significant shifts in CDOM and FDOM signatures among samples consistent with photochemical processing of soil water DOM exported to sunlit surface waters. Indeed, the observed differences between pool surface and bottom waters were largely consistent with shifts in CDOM and FDOM detected following experimental photodegradation of pool bottom waters. CDOM was found to be the main UV light absorbing constituent, accounting for 86 % of UV sunlight attenuation on average. Thus, given that sunlight attenuation by CDOM contributes to the stratification in this system, CDOM absorption sets up a feedback whereby CDOM in the surface layers experiences greater photoexposure, allowing for extensive photodegradation of DOM, while DOM in pool bottom waters is protected from photodegradation.

INTRODUCTION

Dissolved organic matter (DOM) is arguably the most important pool of carbon (C) on Earth. It is the largest C pool in the ocean (Sarmiento and Sundquist, 1992), similar in size to the amount of C in the atmosphere. DOM is also the largest flux of organic C from land to oceans worldwide (Cauwet, 2002; Schlesinger and Melack, 1981). Despite its relatively refractory mean nature and age (mean age ~1000 years), some DOM fractions are highly reactive and each year the conversion of DOM to carbon dioxide (CO_2) accounts for as much CO_2 released from inland waters to the atmosphere as the net ocean absorption from the atmosphere (Battin et al., 2009; Cole et al., 2007). DOM from land is thus a critical intermediate in the global C cycle. When DOM enters aquatic systems it meets one of three fates: (1) complete oxidation to CO_2 and carbon monoxide, (2) partial oxidation to compounds that may be biogeochemically labile or recalcitrant and subsequent transport to marine systems, or (3) conversion to particulate organic matter by flocculation or incorporation into microbial biomass, followed by sedimentation and burial. Of these fates, complete and partial oxidation of DOM by sunlight and microorganisms to CO_2 or to DOM exported to the ocean are dominant. What controls the relative magnitudes of these two pathways is poorly known, but both pathways have important implications for C budgets.

Transfers of C from soils to surface waters are especially strong in the Arctic (Kling et al., 1991), where soils currently store twice the C found in the atmosphere (Ping et al., 2008; Tarnocai et al., 2009) and where C fluxes from surface waters to the atmosphere and from land to ocean could represent up to 40 % of the net land-atmosphere C exchange (maximum flux of approximately 0.16 Pg C y^{-1} and a net

terrestrial sink of 0.4 ± 0.4 Pg C y^{-1}; McGuire et al., 2009). Recent work has shown that photodegradation of DOM from arctic soils can increase the microbial processing of DOM by more than 40 % (Cory et al., 2013). Therefore, rates of DOM photodegradation are critical to understand the impact of thawing arctic soil C on greenhouse gases sources from the Arctic that may create a positive feedback on global warming (Schuur et al., 2008; Serreze and Francis, 2006).

Rates and extent of DOM photodegradation depend on its exposure history and residence time in sunlit surface waters (Cory et al., 2007, 2013; Miller et al., 2009b). Residence time in sunlit surface layers depends on light attenuation of the water column, stratification, and water transit time. The residence time of DOM in sunlit surface is also influenced by storage within hillslope, riparian, and transient zones, which includes in-channel and hyporheic storage (e.g., Bencala and Walters, 1983; McGlynn et al., 1999; McGuire et al., 2007; McNamara et al., 1998; Morrice et al., 1997; Mulholland et al., 1990; Stieglitz et al., 2003). The balance of sunlit surface exposure vs. storage in dark areas may be particularly important for DOM fate in tundra environments (e.g., Brooks and Williams, 1999; McNamara et al., 2008), where headwater streams are shallow (high light exposure) and underlain with permafrost.

For example, Merck et al. (2012) showed differences in DOM quantity and quality between bottom and surface waters of a beaded stream in the Alaskan Arctic that were consistent with extensive photodegradation of DOM in the surface waters. Specifically, they investigated the fluorescent fraction of DOM (FDOM), and reported decreased fluorescence intensities and shifts in FDOM quality in the surface waters compared to bottom waters that are consistent with DOM photodegradation (Cory et al.,

2007). They attributed DOM photodegradation in the surface waters to increased in-pool storage due to strong stratification in the pools. They hypothesized that absorption of solar radiation by DOM was a key factor contributing to stratification because sunlight is rapidly attenuated in waters with high chromophoric DOM (CDOM), restricting the warming of water by solar radiation to the surface layers. The consistent separation of surface and bottom water masses in each pool of the beaded stream results in increased travel times through beaded streams in arctic watersheds, thus affecting the evolution of DOM chemistry and its downstream export.

However, although FDOM has been used as a tracer for DOM source and its photo-exposure history (e.g., Cory et al., 2007), most of this work has been conducted on isolated fractions of DOM or on DOM in low-iron waters (e.g., Biddanda and Cotner, 2003; Miller et al., 2009b). High dissolved iron concentrations in surface waters of the Alaskan Arctic due to export of reduced ferrous iron from soil waters (e.g., Lipson et al., 2010, 2012) may complicate the interpretations of DOM source and degradation along soil flowpaths and in streams. This is because iron can quench DOM fluorescence (Pullin et al., 2007), thereby directly altering the FDOM signature. Alternatively, oxidation of ferrous iron in surface waters may lead to adsorption and subsequent precipitation of DOM (Pullin et al., 2004), which has been suggested to alter DOM quality in a manner similar to DOM photodegradation.

In addition, while CDOM is the main UV and PAR light absorbing constituent in most natural waters (Fee et al., 1996), other dissolved constituents or particles may contribute to light absorption. For example, dissolved iron and iron-containing particles absorb UV and visible light (e.g., Pullin and Cabaniss, 2003b; Pullin et al., 2007;

Weishaar et al., 2003) and may thus contribute to light attenuation. While Gareis (2010) suggested that CDOM was important for light absorption and attenuation in Arctic lakes of the Mackenzie Delta, the role of CDOM in light absorption in high-iron waters has not been investigated.

Thus, to expand on the Merck et al. (2012) findings that suggested a feedback between absorption of sunlight by DOM in beaded streams leading to extensive photodegradation of DOM in sunlit surface waters, I investigated (1) the role of DOM in sunlight attenuation in beaded streams, (2) whether photodegradation could account for the differences in DOM quality previously observed between surface and bottom waters, and (3) the influence of iron on CDOM and FDOM quantity and quality.

SITE DESCRIPTION

Imnavait Creek is a headwater beaded stream located on the North Slope of Alaska in a glacial valley formed during the Sagavanirktok glaciation in the Kuparuk River basin at latitude 68.616 °N and longitude 149.318 °W (Detterman et al., 1958; Hamilton, 1986). The creek primarily lies in the organic soil layer and only occasionally cuts through to the mineral soil (McNamara et al., 1998). The connected pools, or beads, were formed by the erosion and melting of large ice deposits that had underlain the creek (McNamara et al., 1998; Walker et al., 1989).

Water enters Imnavait Creek from melt and associated runoff of snow pack and frozen soil as well as from precipitation events, with snowmelt dominating inputs in the spring (Kane et al., 1989). Previous studies of Imnavait Creek have found that spring snowmelt associated streamflow accounts for 23 to 71 % (Kane et al., 2004) and 32 to 75 % (McNamara et al., 2008) of the watershed's annual water flux compared to 6 to 9 %

produced by the largest summer storm events (McNamara et al., 2008). Runoff travels both overland and through the subsurface, especially through water tracks that occur along the hillslope. The water paths are limited to the active layer as the region is underlain with up to several hundred meters of permafrost, which effectively separates the active layer from any deep ground waters (Osterkamp and Payne, 1981). Previous studies found typical seasonally thawed active layer depths at this site ranged from 25 to 40 cm, occasionally extending to 100 cm (Hinzman et al., 1991); this is consistent with thaw depths measured in this study, which ranged from 13 to 81 cm. Inputs from the riparian zone occur through both surface flow and diffuse subsurface flow (Kane et al., 2000). In addition to connecting chutes, water travels between pools through side tracks with both subsurface flow through the active layer and above surface flow during high water events (Merck et al., 2011).

I studied an approximately 120 m reach of the creek consisting of a series of seven pools connected by short chutes. Pools were named starting with pool 1 and proceeding downstream sequentially to pool 7. Pool surface areas ranged from 2 to 129 m^2 and volumes ranged from 0.1 to 102 m^3. Along the reach of creek studied, one water track drains from the adjacent eastern hillslope, referred to as water track 8.

METHODS

Weather

Air temperature 1 m above the ground and precipitation were measured hourly at a meteorological station on the west-facing ridge of the Imnavait Creek basin approximately 1 km upstream of the study site using a temperature probe (model HMP45C; Campbell® Scientific, Logan, UT) and tipping bucket rain gauge, respectively

(Kane and Hinzman, 2011). UVA and UVB solar radiation were measured at 5 min intervals at Toolik Field Station (TFS) located approximately 11 km west of Imnavait Creek with pyranometers (UVA-1 and UVB-1; Yankee Environmental System, Turner Falls, MA).

Sunlight attenuation

Light attenuation with depth was measured in pools 1, 2, 3, and 6 on 28 June, 2011 using a compact optical profiling system for UV light in natural waters (UV C-OPS; Biospherical Instruments Inc., San Diego, CA). The C-OPS measured downwelling cosine-corrected irradiance at 7 wavebands (305, 313, 320, 340, 380, 395, and 412 nm) and photosynthetically active radiation (PAR). Attenuation coefficients ($K_{d,\lambda}$) were calculated from the downwelling irradiance (E_λ) as a function of depth (z) at each waveband:

$$E_{\lambda,z} = E_{\lambda,0} e^{-K_{d,\lambda} z} \qquad (1)$$

Based on multiple casts in each pool (n = 1 to 5), the coefficient of variation of $K_{d,\lambda}$ ranged from 1 to 3 % in the UV and 9 % for PAR. Means ± standard deviation (SD) of $K_{d,\lambda}$ are reported unless otherwise noted.

In-situ monitoring

Temperature sensor arrays (HOBO® Water Temp Pro v2; Onset Computer Corporation, Inc., Bourne, MA) were deployed vertically in each pool (n = 1 to 5 per pool) from late-June through mid-August, 2011 measuring at 5 minute intervals. The probes were wrapped with aluminum foil to prevent radiation-caused heating (Neilson et al., 2010) and placed starting 10 to 15 cm from the bottom of the pool and then at intervals ranging from 15 to 50 cm up to near the surface. Additionally, intensive

monitoring of pool 2 was conducted for one week in July, 2011 consisting of two sondes deployed near the surface and bottom of the pool with oxygen, pH, specific conductance, and temperature probes (YSI 6920 V2 sonde with ROX™ optical dissolved oxygen, 6561 pH, 6560 conductivity, and 6560 temperature sensors; YSI Inc., Yellow Springs, OH) measuring in-situ at 15 minute intervals.

Sampling

Water samples were collected from the surface and bottom of the seven consecutive pools monthly from June through August, 2011, soil water was collected from water track 8 once in June and twice each in July and August, 2011, and soil water was collected from an array of sites on eastern hillslope adjacent to the study pools monthly from June through August, 2011. Temperature, conductivity, and pH of each sample from pools and water track 8 were measured at the time of collection using WTW meters (models 3210; Xylem, White Plains, NY). Pool water was collected from the surface and bottom of each pool through MasterFlex® tubing (Cole-Parmer, Vernon Hills, IL) using a peristaltic pump (GeoPump Inc., Medina, NY). Seventeen sites were sampled along water track 8 from the hill top to the valley bottom along the creek; the distance between sites ranged from 30 to 190 m. A grid of 55 soil water sites was sampled over a 150 m by 90 m area of the hillslope. Soil water was sampled using stainless-steel soil needles inserted into the soil, through MasterFlex® tubing, into plastic syringes that were used to apply gentle suction. All pool and soil water samples were filtered in the field into high-density polyethylene bottles. Aliquots for analysis of DOM quantity and quality and total dissolved iron via ferrozine assay were filtered through pre-combusted Whatman GF/F glass fiber filters (Whatman, Clifton, NJ) and aliquots for total dissolved

iron analysis via inductively coupled plasma optical emission spectrometer (ICP-OES) were filtered through 0.45 μm polypropylene filters (Whatman). Filtering introduced air into water samples collected from anoxic pool bottom or soil waters.

DOM quantity and quality

Dissolved organic carbon (DOC) samples were acidified with trace-metal grade hydrochloric acid (TMG HCl) to approximately pH 2 to 3 after filtration and stored in the dark at 4 °C until analysis using a high-temperature platinum-catalyzed combustion followed by infrared detection of CO_2 (Shimadzu TOC-5000; Shimadzu, Columbia, MD).

The chromophoric and fluorescent fractions of DOM (CDOM and FDOM, respectively) were analyzed within hours to at most several days of collection. Samples were stored in the dark at 4 ºC until warmed to room temperature (20 to 25 °C) just prior to analysis.

UV-Vis absorbance spectra of CDOM were collected using 1-cm path length quartz cuvettes with a spectrophotometer (USB 2000+UV-VIS; Ocean Optics, Inc., Dunedin, FL). Sample absorption was measured against laboratory-grade deionized (DI) water blanks (Barnstead E-Pure and B-Pure; Barnstead Thermolyne, Dubuque, IA). The spectral slope ratio (S_R) was calculated from the absorbance spectrum of each sample as the ratio of the slope from 275 to 295 nm to the slope from 350 to 400 nm following Helms et al. (2008). CDOM absorption coefficients ($a_{CDOM,\lambda}$) were calculated as follows:

$$a_{CDOM,\lambda} = \frac{A_\lambda}{l} 2.303 \qquad (2)$$

where A is the absorbance reading at wavelength λ and l is the pathlength in meters. $SUVA_{254}$ was calculated following Weishaar et al. (2003) as absorbance at 254 nm

divided by the cuvette pathlength (m) and then divided by the DOC concentration (mg C L^{-1}).

Excitation-emission matrices (EEMs) were measured on all water samples with a Fluoromax-4 fluorometer (Horiba Scientific, Edison, NJ) following the procedures of Cory et al. (2010). An aliquot of sample was placed in the 1-cm quartz cuvette for each EEM and diluted with DI if necessary to bring $A_{254} < 0.6$. EEMs were corrected for inner-filter effects and for instrument-specific excitation and emission corrections in Matlab (version 7.7) following Cory et al. (2010). The fluorescence index (FI; McKnight et al., 2001) was calculated from each corrected EEM as the ratio of emission intensity at 470 nm over the emission intensity at 520 nm at an excitation wavelength of 370 nm (Cory et al., 2010). Emission intensity at FDOM peaks A, C, and T was evaluated at excitation/emission pairs 250/450, 350/450, 275/340 (nm/nm), respectively, in RU (Coble et al., 1990). Mean ± SD are reported unless otherwise noted.

Total dissolved iron

ICP-OES

Aliquots of filtered water were acidified to pH 2 to 3 with TMG HCl and stored in the dark at 4 °C until analysis using an ICP-OES (Perkin Elmer Optima 4300DV; Perkin Elmer Inc., Waltham, MA). Concentrations were calculated using a calibration curve made from serial dilutions of a standard mix (High-Purity Standards; Charleston, SC). Soil water samples from the hillslope were not analyzed via ICP-OES. Mean ± SD are reported unless otherwise noted.

Ferrozine assay

Aliquots of filtered water were shipped to the laboratory in Chapel Hill, North Carolina for iron analysis. Total time between collection and analysis ranged from two weeks to two months. Samples were stored at 4 °C until analysis, but were not acidified. Although oxidation of ferrous iron is expected to be slower in the acidic water of Imnavait Creek (mean pH = 5.8 ± 0.5) compared to near-neutral waters (Pullin and Cabaniss, 2003a; Stumm and Lee, 1961), it is likely that the dissolved total iron concentration measured in the lab were lower than field values due to oxidation of ferrous iron and precipitation of ferric iron.

Total iron was quantified on all samples using the ferrozine assay (Stookey, 1970). Briefly, 2 mL of sample was reduced via the addition of 200 µL of 6.25 M hydroxylamine hydrochloride and then reacted with 100 µL of 15 mM ferrozine in 15 mM HEPES buffer (pH 7) for 45 minutes prior to measuring the absorbance at 562 nm. Absorbance of the sample solution plus ferrozine-ferrous iron complex was corrected for the absorbance of CDOM at 562 nm. The concentration of iron was calculated using a nine-point calibration curve consisting of similarly analyzed solutions of ferrous ammonium sulfate (0 to 50 µM in 0.01 M TMG HCl). Samples exceeding 50 µM were diluted with DI at the time of analysis. Mean ± SD are reported unless otherwise noted.

Effects of iron on CDOM and FDOM

Filtered soil water samples were reacted with a non-fluorescent iron ligand (deferoxamine mesylate, DFB) to competitively scavenge iron from complexes with the natural DOM in order to evaluate the effects of iron on CDOM and FDOM signals. Samples were filtered at the time of collection through pre-combusted GF/F filters and

stored in the dark at 4 °C prior to experimentation. A stock solution of 0.22 mM DFB in DI was prepared immediately prior to addition to samples. DFB was added to an aliquot of each sample to achieve a molar ratio of 0.2 DFB to total dissolved iron measured via ferrozine assay. Controls consisted of sample plus DI providing the same dilution. DFB reacted samples and DI controls were allowed to equilibrate for 48 hours at room temperature in the dark and then subsamples were analyzed for CDOM, FDOM, and total dissolved iron via ferrozine assay as described above.

DOM photodegradation

Pool bottom water collected in amber HDPE bottles in the field was brought back to TFS for photochemical degradation experiments as described in Cory et al. (2013). Briefly, four replicates of GF/F-filtered water samples placed in 12-mL pre-combusted borosilicate Exetainer® vials (Labco Ltd.; Ceredigion, UK) were exposed to natural sunlight for 12 hours alongside four foil-wrapped dark control vials at temperatures ranging from 10 to 16 °C. Although borosilicate glass is not as UV transparent as quartz the difference is quite small for light from 280 through 400 nm, 83 vs. 86 percent transmittance respectively (Miller et al., 2009a). After exposure to light, subsamples were analyzed for CDOM and FDOM as described above. Changes in DOM quality are reported as mean ± standard error (SE) unless otherwise noted.

RESULTS

Weather patterns

Average daily peak solar radiation was 38 W m^{-2} in the UVA and 1.3 W m^{-2} in the UVB. Air temperature ranged from -2 to 19 °C, with a mean of 8.7 °C. Solar radiation and temperature both exhibited diel fluctuations during the study period of June through

August, 2011 (Fig. 1.1). Four precipitation events exceeded 2 mm of water per hour and a total of 7.4 cm of precipitation occurred at Imnavait during the study period (Fig. 1.1).

Physical characteristics of Imnavait Creek

Pools 2, 3, 5, 6, and 7 were thermally stratified on 43 to 46 out of 50 days investigated in the summer of 2011, where stratification was quantified as layers of continuously different temperature water (Fig. 1.2). Pools 1 and 4 did not exhibit the same stratification patterns observed in pools 2, 3, 5, 6, and 7. Pool 1 mixed daily and the shallow depth of pool 4 (0.2 m) in comparison to the mean depths of other pools (1.5 m) likely prevented stratification.

The regularly stratified pools (2, 3, 5, 6, and 7) mixed within hours after a precipitation event on 17 July, 2011 (Fig. 1.1 and 1.2). Temperature profiles of the pools show that re-stratification occurred within four to five days following the initial precipitation-driven mixing event (Fig. 1.2).

UV attenuation coefficients, $K_{d,\lambda}$, decreased exponentially with increasing wavelength, ranging from 88 ± 12 m^{-1} at 305 nm to 17 ± 3 m^{-1} at 412 nm. PAR attenuation coefficients were 3 ± 1 m^{-1}. Thus the depth of 1% surface irradiance ($z_{1\%}$) was < 8 cm in the UVB and 6 to 27 cm in the UVA range. PAR penetrated deepest in the water column, with $z_{1\%}$ up to 1.8 m. Given that the depth of pools in which sunlight attenuation was measured ranged from 1.0 to 1.6 m and the bathymetry of the pools, 8 to 12 % of the water volume of each pool received UVB light, 28 to 37 % of the water volume of each pool received UVA light, and pool water at all depths received PAR light.

$K_{d,\lambda}$ in the UVB was strongly positively correlated with DOC concentrations in Imnavait Creek pools ($r^2 \geq 0.80$, $p \leq 0.10$, n = 4 pools; data not shown). $K_{d,\lambda}$ was also strongly positively correlated with $a_{CDOM,\lambda}$ at all wavelengths measured except 380 nm, ($r^2 \geq 0.81$, $p \leq 0.10$, n = 4 pools; Fig. 1.3a). On average $a_{CDOM,\lambda}$ was 84 % of $K_{d,\lambda}$ in the UVB compared to 88 % in the UVA. Differences between $a_{CDOM,\lambda}$ measured on filtered water using a UV-Vis spectrophotometer, and in-situ $K_{d,\lambda}$ varied by wavelength (Fig. 1.3a). For example, differences between $a_{CDOM,\lambda}$ and $K_{d,\lambda}$ were smaller in the UVA compared to the UVB (Fig. 1.3a).

$K_{d,\lambda}$ was strongly positively correlated with concentrations of total dissolved iron at all wavelengths measured except PAR, ($r^2 \geq 0.85$, $p < 0.10$, n = 4 pools; Fig. 1.3b). The slope of $K_{d,\lambda}$ vs. total iron was greater at lower wavelengths (305 to 380 nm) in contrast to small changes in $K_{d,\lambda}$ with increasing iron concentration at 395 and 412 nm and PAR (Fig. 1.3b). However, likely due to the small sample size for $K_{d,\lambda}$ (n = 4 pools), there were no significant differences in the slopes of the correlations between $K_{d,\lambda}$ and total dissolved iron.

Soil water

Water track 8

Water track 8 soil water samples had a mean conductivity of 26 ± 14 µS, mean pH was 5.2. Water track 8 soil water DOC concentrations ranged from 493 to 4953 µM C with a mean of 1357 ± 818 µM C (Table 1). The mean CDOM absorption coefficient at 320 nm ($a_{CDOM,320}$), a measure of the concentration of CDOM, was 60 ± 44 m^{-1}. Mean $SUVA_{254}$, a proxy for DOM aromaticity (Weishaar et al., 2003), was 4.4 ± 0.9 m^{-1} (mg C $L^{-1})^{-1}$. Mean slope ratio (S_R), a proxy for average molecular weight of the DOM (Helms

et al., 2008), was 0.75 ± 0.08. Mean fluorescence index (FI), a proxy for aromaticity of the fulvic acid fraction (McKnight et al., 2001) or photo-processing (Cory et al., 2007), was 1.49 ± 0.05.

Analysis of FDOM provides insight into three types of carbon within the DOM pool: carbon associated with terrigenous or microbial source material (peaks A and C) and carbon associated with free or combined fluorescent amino acids (peak T), specifically tryptophan, tyrosine, and phenylalanine (Coble et al., 1990; representative EEM shown in Fig. 1.4). The mean peak A intensity for water track 8 soil water was 2.2 ± 1.2 RU. The mean ratio of FDOM intensities at peaks C and A (C/A) was 0.54 ± 0.05 and the mean ratio of peaks T and A (T/A) was 0.14 ± 0.05.

There was overlap in both the range and mean concentration of total dissolved iron in the water track soil water measured by ICP-OES and the colorimetric ferrozine assay (Table 1). The water track 8 soil water concentrations of total dissolved iron measured via ICP-OES ranged from 2 to 107 μM with a mean concentration of 26 ± 26 μM. Concentrations of total dissolved iron measured via ferrozine assay ranged from 1 to 111 μM with a mean of 24 ± 29 μM.

Hillslope soil waters

Hillslope soil water DOC concentrations ranged from 442 to 6881 μM C with a mean of 1882 ± 1206 μM C (Table 1). Mean $a_{CDOM,320}$ was 169 ± 165 m^{-1}. Mean $SUVA_{254}$ was 6 ± 2 m^{-1} (mg C L^{-1})$^{-1}$. Mean S_R of hillslope soil water was 0.69 ± 0.10 and mean FI was 1.52 ± 0.04. Mean FDOM intensity at peak A was 2.6 ± 1.6 RU. The mean ratio of FDOM intensities C/A was 0.62 ± 0.06 and the mean ratio of T/A was 0.19 ± 0.07 (representative EEM in Fig. 1.4). Total dissolved iron concentrations in the

hillslope soil waters measured via ferrozine assay ranged from < 1 to 563 μM with a mean of 96 ± 103 μM.

Pool bottom water

When stratified, pool bottom waters had an average conductivity of 37 ± 30 μS cm^{-1} and average pH of 5.5. The bottom water of pool 2 was always anoxic when stratified based on week-long in-situ probe data collected in July, 2011 during stratified conditions (supporting information Fig. 1.1).

The mean concentration of DOC in the pool bottom water was 1252 ± 362 μM C. Mean $a_{CDOM,320}$ was 78 ± 56 m^{-1} (Table 1). Mean $SUVA_{254}$ was 5 ± 2 m^{-1} (mg C L^{-1})$^{-1}$. Mean S_R of the pool bottom water was 0.70 ± 0.08 and mean FI was 1.45 ± 0.04. Mean bottom water FDOM intensity at peak A was 2.4 ± 0.5 RU. The mean ratio of FDOM intensities C/A was 0.49 ± 0.04 and the mean ratio of T/A was 0.13 ± 0.04 (representative EEMs in Fig. 1.4).

There was overlap in both the range and mean concentration of total dissolved iron in the pool bottom waters measured by ICP-OES and the colorimetric ferrozine assay (Table 1). Total dissolved iron concentrations in the pool bottom waters measured via ICP-OES ranged from 4 to 114 μM, with a mean of 39 ± 33 μM. Total dissolved iron concentrations measured via ferrozine assay ranged from 3 to 87 μM with a mean of 28 ± 28 μM.

Pool surface water

The pool surface waters had an average conductivity of 13 ± 2 μS cm^{-1} and average pH of 5.7. The mean concentration of DOC in the pool surface waters was 785 ± 60 μM C. The mean $a_{CDOM,320}$ was 34 ± 5 m^{-1} (Table 1). Mean $SUVA_{254}$ was 4.5 ± 0.5

m^{-1} (mg C L^{-1})$^{-1}$. Mean S_R of DOM in the surface waters was 0.78 ± 0.08 and mean FI was 1.41 ± 0.03. Mean surface water FDOM intensity at peak A was 1.2 ± 0.2 RU. The mean ratio of FDOM intensities at peaks C and A was 0.45 ± 0.02 and the mean ratio of peaks T and A was 0.12 ± 0.01 (representative EEMs in Fig. 1.4).

The range of total dissolved iron concentrations in the water track soil water measured by ICP-OES and the colorimetric ferrozine assay overlapped but the mean concentrations as measured by the two methods were significantly different (;Table 1). Total dissolved iron concentrations in pool surface waters measured via ICP-OES ranged from 4 to 46 μM with a mean of 21 ± 10 μM. Total dissolved iron measured via ferrozine assay ranged from 2 to 7 μM with a mean of 4 ± 1 μM.

Effect of stratification on pool chemistry

High temporal resolution data collected under stratified conditions (i.e., no mixing events occurred) in pool 2 from 8 to 15 July, 2011 showed strong differences in conductivity, pH, and dissolved oxygen (DO) between surface and bottom pool water in Imnavait Creek. During this period of strong stratification, the specific conductance of the surface water was significantly greater than the bottom water (paired t-test, $p < 0.01$) with mean values of 13 and 25 μS cm^{-1}, respectively. Likewise, the pH was significantly higher in the surface water compared to bottom water (paired t-test, $p < 0.01$) with mean values of 5.8 vs. 5.4, respectively. The surface water DO concentration exhibited diel fluctuation but was consistently well oxygenated throughout this period; percent saturation ranged from 73 to 95 %, with a mean concentration of 240 μM O_2. The DO of the bottom water was consistently less than 3 μM after the initial stabilization (supporting

information Fig. 1.1). The concentration of DO in the surface water was significantly greater than the bottom waters (paired t-test, $p < 0.01$).

Stratified pools exhibited large differences in DOM quantity and quality. For example on 14 July, 2011, DOC concentrations were up to three times higher in pool bottom waters compared to the surface (Fig. 1.5). In contrast, mixed pool 1 had similar DOM quantity and quality in surface and bottom waters (Fig. 1.5). Stratified pool bottom waters also had significantly greater levels of CDOM and FDOM compared to surface waters (paired t-test, $p < 0.01$; Fig. 1.5). In addition, stratified pools exhibited differences in DOM quality. For example, surface waters almost always had significantly lower $SUVA_{254}$ (paired t-test, $p < 0.05$; supporting information Fig. 1.2), significantly higher S_R (paired t-test, $p < 0.01$; supporting information Fig. 1.3), and significantly lower FI compared to bottom waters (paired t-test, $p < 0.01$; Fig. 1.5). There was no significant difference in $SUVA_{254}$, S_R, or FI in mixed pool 1 on 14 July, 2011. Stratified pool 7 also had no significant depth difference in $SUVA_{254}$. Stratified pool 7 had lower S_R in the surface compared to bottom waters, which is the only pool sampled on any date with lower S_R in the surface compared to the bottom waters.

Total dissolved iron had similar patterns to the observed depth differences in DOC, CDOM, and FDOM: total dissolved iron was significantly higher in pool bottom waters compared to pool surface waters (paired t-test, $p < 0.05$; Table 1) except in mixed pool 1 where similar concentrations were observed in the surface and bottom waters. Concentrations of total dissolved iron were correlated with concentrations of DOM quantity (DOC, Pearson's $r = 0.93$) and quality (e.g., FI, Pearson's $r = 0.80$) in pool waters.

DOM quality and quantity and total dissolved iron concentrations were similar between different pool surface waters throughout the summer of 2011, in contrast to the variability as measured by SD in bottom water values over the season (Table 1). For example on 14 July, 2011, the average surface water DOC across all pools was 723 ± 23 μM C, while the average bottom water DOC was 1305 ± 415 μM C. $a_{CDOM,320}$ exhibited similar patterns, with a mean of 47 ± 3 m^{-1} in pool surface waters compared to higher mean and larger variability in pool bottom waters, 119 ± 87 m^{-1}. Mean $SUVA_{254}$ was 4.9 ± 0.2 m^{-1} (mg C L^{-1})$^{-1}$ in the pool surface waters compared to 6 ± 2 m^{-1} (mg C L^{-1})$^{-1}$ in the pool bottom waters. Likewise, total iron concentrations on 14 July, 2011 were lower and less variable in pool surface waters, 3.2 ± 0.4 μM, compared to bottom waters, 26 ± 31 μM.

After the pools mixed on 17 July, 2011 (Fig. 1.1), the temperature data show that the pools began to re-stratify on 21 through 23 July, 2011 (Fig. 1.1). The direction and magnitude of the depth differences in DOM quantity and quality and in iron concentration in Imnavait pool water sampled on 4 August, 2011, two weeks after the mixing event and the onset of re-stratification, were similar to the depth differences measured in the pools just prior to the mixing event (14 July, 2011; Fig. 1.5).

Effects of iron on CDOM and FDOM

Dissolved iron and its complexes absorb UV and visible light thus resulting in higher $a_{CDOM,\lambda}$ and $SUVA_{254}$ than expected based on DOC concentrations alone (Weishaar et al., 2003). In addition, dissolved iron alters FDOM signals because iron quenches DOM fluorescence non-uniformly as a function of wavelength (Pullin et al., 2007). A non-fluorescent iron ligand (deferoxamine mesylate, DFB) was added to soil

water samples to competitively scavenge iron from complexes with the natural DOM to evaluate the effects of iron on CDOM and FDOM. Addition of DFB decreased the ferrozine-accessible iron by 27 ± 5 %. If the iron bound by DFB (measured as iron no longer accessible by ferrozine) had been associated with CDOM and FDOM, the expectation was that complexation by DFB would result in significant shifts in CDOM or FDOM quality and/or quantity.

There was no significant difference in $a_{CDOM,254}$ of samples with and without the addition of DFB (t-test, $p > 0.05$). DFB itself is weakly absorbing, $a_{254} \leq 0.1$ m^{-1} in DI at concentrations added to soil water samples compared to $a_{254} \geq 100$ m^{-1} of unaltered soil waters and therefore is not expected to significantly alter absorbance measurements.

As expected based on previous work (Pullin et al., 2007), the addition of DFB to soil waters from Imnavait Creek reduced iron quenching of fluorescence and increased FDOM peak intensities. Addition of DFB to soil waters resulted in a significant increase in fluorescence intensity at peaks A, C, and T (t-test, $p \leq 0.05$). The fluorescence intensity of peak A increased by 10 ± 4 %, peak C increased by 5 ± 2 %, and peak T increased by 7 ± 4 % compared to samples without DFB; these changes in fluorescence intensity were not explained by changes in absorbance which was approximately 1 %. Because there was no significant difference in iron's capacity to quench peaks A, C or T, there was no detectable influence of iron on the ratios of peaks C/A or T/A compared to the ratios in samples without DFB. Further, there was no significant change in FI after addition of DFB compared to samples not reacted with DFB (t-test, $p > 0.05$). There was no detectable fluorescence in solutions of DFB in DI.

Photodegradation of DOM in Imnavait Creek water

Exposure of Imnavait Creek DOM to 12 hours of sunlight resulted in significant loss of CDOM and FDOM compared to dark controls (paired t-tests, $p < 0.05$; Table 2); on average there was a 9 % decrease in CDOM and FDOM (depending on wavelength). Photobleaching resulted in a significant increase in S_R (from $0.74 \pm < 0.01$ to $0.87 \pm < 0.01$) and a significant decrease in the FI (from $1.55 \pm < 0.01$ to $1.35 \pm < 0.01$). There was a preferential loss of fluorescence at peak C compared to loss of intensity for peaks A or T upon exposure to sunlight. For example, peak C decreased by $26 \pm < 1$ %, peak A decreased by 11 ± 1 %, and the fluorescent intensity of peak T increased by 5 ± 2 % after exposure to sunlight. This preferential loss of fluorescence resulted in a significant shift in the ratio of the fluorescent intensity of C/A from $0.53 \pm < 0.01$ to $0.44 \pm < 0.01$ (t-test, $p < 0.05$) and a significant shift in the ratio of the fluorescent intensity of T/A from $0.09 \pm < 0.01$ to $0.11 \pm < 0.01$ (t-test, $p < 0.05$). Sunlight exposure also resulted in a significant blue-shift of the excitation and emission maxima of peaks A and C, i.e., shifted to lower wavelengths. For example, for photo-exposed DOM the excitation position of peak C was blue-shifted to lower wavelengths by 13 ± 3 nm (t-test, $p < 0.05$) and the emission peak was shifted to lower wavelengths by 6 ± 1 nm (t-test, $p < 0.05$) compared to dark controls.

DISCUSSION

Pool bottom water chemistry driven by soil water inputs

In all measures of water chemistry, pool bottom water more closely resembles soil water than pool surface water suggesting that the source of pool bottom water was primarily inputs of soil water (Merck and Neilson, 2012; Merck et al., 2011) enriched in

DOM and iron compared to surface waters. This is evident from the overlap in pH, conductivity, and concentrations of DOC, CDOM, FDOM, and total dissolved iron between both water track 8 and hillslope soil waters with pool bottom waters (Table 1). In contrast, pH, conductivity, and concentrations of DOC, CDOM, FDOM, and total dissolved iron in pool surface waters were significantly different compared to soil waters and pool bottom waters (Table 1; t-test, $p < 0.05$). Soil water inputs to the pools were also evident based on the similarities of the peak positions and intensities of EEMs of soil water and pool bottom water from a stratified pool (Fig 5; Merck et al., 2011).

Both the soil waters and the pool bottom waters exhibited larger variability in the concentration and quality of dissolved constituents (e.g., Fig. 1.5) both spatially and temporally across the season. It is likely that pool bottom water chemistry depends strongly on soil water inputs, which are affected by flowpaths and inflow volumes. The flowpaths, and thus the sources of soil waters to the different pools, likely change over the season due to shifts in preferential flowpaths along the hillslope and riparian zone. In contrast to the pool bottom waters, the smaller range of concentrations and quality of dissolved constituents across the pool surfaces suggest that the surface waters of the pools are connected and well-mixed (Table 1; Fig. 1.5). This mixing is highlighted by the fact that surface waters may stratify daily but tend to mix at night (Fig. 1.2).

The high variability observed in the pool bottom water chemistry (Fig. 1.5; Table 1, based on standard deviations of mean values collected among pools and over time), is likely a reflection of the high variability in soil water chemistry both spatially and seasonally (Table 1, based on standard deviations of mean values collected at different sites on the same day, and at the same sites on different days). For example, the

variability observed at soil water sites located at the bottom of the hillslope, measured as standard deviation of each site sampled repeatedly during the study period, overlapped the range of standard deviation of all soil water sites at the bottom of the hillslope for each specific sampling date for DOC, $a_{CDOM,320}$, $SUVA_{254}$, S_R, peak A, FI, and Fe. In other words, the range of variability in concentrations observed at a given site across all sampling dates overlapped with the variability on a given sampling date across all those sites overlapped. Thus, both spatial and seasonal variability likely altered the inputs to the pool bottom waters. Despite these variations as well as likely changing flowpaths, soil water inputs still were high in DOC and iron and drove the light attenuation and thereby photo-processing of the pool surface waters and photo-protection of the pool bottom waters.

$a_{CDOM,\lambda}$ is the main UV-light absorbing constituent in Imnavait surface waters

CDOM accounted for most of the UVB and UVA light attenuation in the pools, given that $a_{CDOM,\lambda}$ was 84 to 88 % of $K_{d,\lambda}$ in the UVB and UVA, respectively, consistent with the literature showing that CDOM is the predominant light absorbing constituent in many surface waters (Gareis et al., 2010; Morris et al., 1995). For example across a range of lakes, $a_{CDOM,\lambda}$ accounted for on average 36 and 75 % of $K_{d,\lambda}$ at 305 nm and PAR, respectively (Morris et al., 1995).

$K_{d,\lambda}$ is expected to be larger than or equal to $a_{CDOM,\lambda}$ in all water bodies due to removal of other light absorbing or scattering particles during filtration before $a_{CDOM,\lambda}$ analysis. However, the observations in pool 2 did not follow this expectation and thus fall below the 1:1 line (Fig. 1.3). The larger values of $a_{CDOM,\lambda}$ compared to $K_{d,\lambda}$ in pool 2 are likely due to (1) flocculation after filtration but before $a_{CDOM,\lambda}$ analysis resulting in an

elevated baseline due to scattering or (2) C-OPS measurement error. Only one C-OPS cast was made in pool 2, but the standard error of replicate casts (n = 3 to 5) in the other pools ranged from < 1 to 8 m^{-1} depending on wavelength and pool, representing on average 0.2 to 7.8 % of the average replicate $K_{d,\lambda}$. In pool 2, $a_{CDOM,\lambda}$ was 3.5 to 10.5 % greater than $K_{d,\lambda}$. Thus, measurement error in $K_{d,\lambda}$ could account for most of the observed difference in $K_{d,\lambda}$ and $a_{CDOM,\lambda}$ in pool 2.

Previous work has found that DOM increases the solubility of iron, likely due to the formation of iron-DOM complexes (Luther III et al., 1992; Maranger and Pullin, 2002; Pullin and Cabaniss, 2003b). Addition of iron to solutions containing DOM isolates can increase absorbance in the visible light range (Pullin et al., 2007), whereas freshly formed colloids of fulvic acid isolates and iron have been found to absorb most strongly in the UV region (Pullin and Cabaniss, 2003a). Thus, the larger increase in light attenuation with increasing iron concentration (i.e., greater slope) in the UVB compared to the UVA region (Fig. 1.3) suggests that organic complexes of iron may be an important factor in UVB light attenuation in Imnavait Creek, in addition to attenuation by particulate iron and other particles not captured by either $a_{CDOM,\lambda}$ or total dissolved iron analyses.

Photodegradation of DOM in surface waters can account for depth differences in DOM quality

Differences in the CDOM and FDOM concentrations of the surface and bottom waters of stratified pools were largely consistent with the effects of photochemical degradation on CDOM and FDOM. Photo-exposure of bottom water resulted in loss of CDOM and FDOM, and increased S_R, decreased FI, decreased ratio of peak C to A, and a

small but significant increase in the ratio of peak T to A compared to dark controls. Similarly, pool surface waters had lower CDOM and FDOM concentrations, higher S_R, lower FI, and a lower ratio of peak C to A, but, no significant difference in the ratio of peak T to A compared to pool bottom waters. These results suggest that photochemical reactions may be important controls on the differences observed between surface and bottom waters in stratified pools.

One difference in FDOM quality between surface and bottom waters not explained by DOM photodegradation was the ratio of peak T to A. This ratio, which is a proxy for the labile fraction of DOM (Cory and Kaplan, 2012 and references therein), increased after experimental photo-exposure consistent with previous work showing that photodegradation increases the ratio of amino acid-like to terrestrial DOM (Cory et al., 2007), but there was no significant difference in the ratio of T/A between pool surface and bottom waters. A lack of observed difference in T/A between surface and bottom waters could be due to rapid use of the more labile fraction of DOM in the surface following photodegradation (Cory et al., 2013), thus minimizing the photochemical fingerprint of increased T/A ratio of the FDOM.

Assessing the influence of iron on CDOM and FDOM

Despite the lack of detectable change in $a_{CDOM,\lambda}$ upon addition of DFB, at the average total dissolved iron and DOC concentrations of soil water samples from Imnavait we estimate that UV light absorption by free or complexed iron may increase $SUVA_{254}$ by 0.8 to 1.8 m^{-1} (mg C $L^{-1})^{-1}$ compared to 0.5 to 0.8 m^{-1} (mg C $L^{-1})^{-1}$ in pool surface waters and 1.0 to 1.3 L mg C^{-1} m^{-1} in pool bottom waters using the relationship developed by Weishaar et al. (2003); however, the magnitude likely depends on the nature of the

iron-organic ligand. Using the average measured values of $SUVA_{254}$ in the surface and bottom waters of Imnavait Creek pools (Table 1) and the relationship between $SUVA_{254}$ and aromaticity developed by Weishaar et al. (2003), we estimated the percent aromatic carbon content of the pool surface and bottom waters as 33 and 36 %, respectively. These values are slightly higher than the 23 % measured on the fulvic acid fraction of Imnavait DOM via ^{13}C-NMR by Cory et al. (2007) given that analytical error is ± 5 % (Kögel-Knabner et al., 1991). DOM in unfractionated whole water likely has an aromatic C content less than or equal to the fulvic acid fraction of DOM (Cory et al., 2007); thus, 23 % is likely a maximum aromatic C content for Imnavait DOM, assuming the DOM collected in previous work is representative of the water in this study. Taken together, the $SUVA_{254}$ based over-estimate of aromatic C is consistent with the presence of iron increasing $a_{CDOM,\lambda}$ and thus $SUVA_{254}$.

DFB strongly and preferentially binds ferric iron (stability constants range from 10^{20} to 10^{50}; Albrecht-Gray and Crumbliss, 1998; Neilands, 1981; Witter et al., 2000) and studies suggest that any loss of ferrous iron actually occurs via initial oxidation to ferric iron followed by binding (e.g., Goodwin and Whitten, 1965). The equilibration time and conditions used in the literature range from 12 hours to 2 weeks and 4 to 20 °C (e.g., Gao and Zepp, 1998; Hammerschmidt and Fitzgerald, 2010; Southworth and Voelker, 2003; White et al., 2003; Xie et al., 2004); we chose a mid-range equilibration time of 48 hours at room temperature. Given that most iron in the samples was likely ferrous iron, and that ferrous iron was relatively stable to oxidation in these low pH waters, it is not surprising that minimal effects of DFB were observed on CDOM and FDOM. Ferrous

iron may be strongly associated with DOM, slowing its oxidation and slowing its competitive complexation with DFB.

Quenching of FDOM by iron likely alters the fluorescence of DOM in all waters sampled from Imnavait Creek, but the observed differences between pool surface and bottom waters are not fully explained by fluorescence quenching alone. The pool surface waters exhibited lower fluorescence at all peaks as well as a lower ratio of peak C to A and no change in the ratio of peak T to A compared to the pool bottom waters. However, quenching of DOM fluorescence would be expected to occur in both the surface and bottom waters due to the presence of iron at both depths (Table 1). The average ratios of DOC to total dissolved iron in the surface and bottom waters are similar when using the iron concentrations measured via ICP-OES (37 vs. 32 μM DOC C per μM Fe, respectively) in the 0.45 μm filter fraction but quite different using the iron concentrations measured via ferrozine assay (196 vs. 45 μM DOC C per μM Fe, respectively) in the 0.7 μm filter fraction. These ratios of DOC to iron are not consistent with iron quenching explaining the lower fluorescence observed in the surface waters because there was equal or greater DOC C per μM iron in the surface waters compared to the bottom waters. If iron quenching was driving the observed differences between the bottom and surface waters we would expect a lower ratio of DOC C to iron in the surface waters. Pullin et al. (2007) found that higher molecular weight DOM is more susceptible to binding with ferric iron than lower molecular weight compounds. Thus we might expect that DOM in the larger size filter fraction would be more susceptible to binding with iron and therefore fluorescence quenching.

The observed increase in fluorescence of soil waters following the addition of iron-ligand DFB shows that iron quenched the fluorescence of DOM in Imnavait Creek waters but did not alter the FI or fluorescence ratios between samples before and after addition of DFB, suggesting that these measures of DOM quality were not altered by the presence of iron. Further, the increase in fluorescence in soil water samples following the addition of DFB (5 to 10 % depending on the peak) was much less than the observed percent difference between pool surface and bottom waters, 30 to 38 % depending on the peak. The patterns of DOM quality between the surface and bottom waters are not consistent with the changes observed in samples equilibrated with DFB.

Iron may play a role in depth differences of DOM chemistry under stratified conditions because adsorption of DOM to iron particles or formation of iron-DOM colloids and subsequent precipitation in oxic surface waters may preferentially remove fractions of DOM (Brinkmann et al., 2003; Gao and Zepp, 1998; Pullin et al., 2004). Pullin et al. (2004) showed that adsorption to iron particles and photochemical degradation both alter DOM chemistry in the same way, such that the net effect of sunlight exposure on DOM in the presence of iron is greater than either process acting alone. Adsorption of photochemically reacted DOM to goethite produced solutions with lower molecular weight and less aromatic DOM than addition of goethite in the dark or photodegradation of DOM in the absence of goethite (Pullin et al., 2004). These processes would be expected to result in an increase in $S_{R,}$ the proxy inversely related to average molecular weight of DOM, and a decrease in $SUVA_{254}$, a proxy for aromaticity, compared to unreacted DOM. Surface waters of Imnavait Creek are well oxygenated, likely resulting in the formation of iron oxy-hydroxides. Thus, it is likely that DOM in

the surface waters of Imnavait Creek is altered by the dual effects of photo-oxidation and adsorption to iron particles. For example, higher S_R in the surface waters suggests lower average molecular weight of the DOM compared to the bottom waters, consistent with fractionation due to adsorption of DOM to goethite, and lower $SUVA_{254}$ in the surface waters compared to the bottom waters suggests lower aromaticity. Although the depth differences are consistent with photochemical degradation of the DOM, the strong gradient in iron and DO between surface and bottom waters likely means that both photo-processing and iron-induced adsorption occur in this system.

CONCLUSIONS

An important consequence of high concentrations of terrestrially-derived CDOM and iron in Imnavait Creek was that nearly all UV light was attenuated within the top layer of water (i.e., $z_{1\%}$ of UV light < 30 cm at all wavelengths) and even PAR light, which reached the bottom of each pool measured, was attenuated by 50 % at 17 to 28 cm. Thus, DOM in the bottom waters was protected by the surface waters from photodegradation. In pools where the water column mixed, all the DOM in the pool was susceptible to photodegradation. The fact that experimental photodegradation of Imnavait DOM reproduces most of the observed differences in CDOM and FDOM quality between surface and bottom waters strongly suggests that the soil water DOM delivered to pool bottom waters in Imnavait Creek is protected from photo-processing. In contrast, the DOM in surface waters is more extensively photodegraded given its greater exposure to sunlight. Interactions between iron and DOM, especially photo-exposed DOM and iron containing particles, may also be important in preferentially removing

specific fractions of DOM from the surface waters and contribute to the observed differences between the bottom and surface waters of stratified pools.

It is also important to recognize that photodegraded DOM is continually mixed with DOM from soils that has no history of light exposure and flushed into surface waters. Thus, to understand the dynamics of DOM degradation in natural systems, short-term kinetic studies which mimic the varied inputs and processing of DOM under natural conditions is the best approach. Finally, to evaluate how changes in climate will alter carbon cycling, experimental studies must be placed into the context of controls at larger, landscape scales. These controls are essentially the water residence time and the total sunlight exposure of the DOM as it moves from lakes and streams on its way to the ocean.

Table 1. Mean and (*standard deviation*) of iron and DOM chemistry by sample location at Imnavait Creek.

	Total Iron [a] FZ [b] (μM)	Total Iron [c] ICP [d] (μM)	DOC [e] (μM C)	$a_{CDOM,320}$ [f,g] (m^{-1})	$SUVA_{254}$ [h,e] (m^{-1} (mg C L^{-1})$^{-1}$)	S_R [i,g]	FI [j,g]	Peak A [g] (RU)	Peak C [g] (RU)	Peak T [g] (RU)
Water track soil water	24 (*29*)	26 (*26*)	1357 *(818)*	60 (*44*)	4.4 (*0.9*)	0.75 (*0.08*)	1.49 (*0.05*)	2.2 *(1.2)*	1.2 *(0.7)*	0.3 (*0.2*)
Hillslope soil water	96 (*103*)	-	1822 (*1206*)	169 (*165*)	6 (*2*)	0.69 (*0.10*)	1.52 (*0.04*)	2.6 (*1.6*)	1.6 (*1.1*)	0.5 (*0.3*)
Pool bottom	28 (*28*)	39 (*33*)	1252 *(362)*	78 (*56*)	5 (*2*)	0.70 (*0.08*)	1.45 (*0.04*)	2.4 *(0.5)*	1.2 *(0.3)*	0.3 (*0.1*)
Pool surface	4 (*1*)	21 (*10*)	785 *(60)*	34 (*5*)	4.5 (*0.5*)	0.78 (*0.08*)	1.41 (*0.03*)	1.7 *(0.2)*	0.75 *(0.08)*	0.19 (*0.02*)

[a] n = 53 for water track 8, 179 for hillslope, 12 for pool bottom, and 14 for pool surface samples
[b] FZ indicates total dissolved iron detected via ferrozine assay
[c] n = 36 for water track 8, 12 for pool bottom, and 14 for pool surface samples
[d] ICP indicates total dissolved iron detected via inductively coupled plasma optical emission spectrometer analysis
[e] n = 55 for water track 8, 144 for hillslope, 18 for pool bottom, and 21 for pool surface samples
[f] $a_{CDOM,320}$ indicates absorption coefficient of CDOM at 320 nm
[g] n = 55 for water track 8, 181 for hillslope, 18 for pool bottom, and 21 for pool surface samples
[h] $SUVA_{254}$ indicates specific UV absorbance at 254 nm
[i] S_R indicates slope ratio
[j] FI indicates fluorescence index

Table 2. Mean percent change and (*standard error*) of DOM chemistry of Imnavait Creek pool bottom waters after exposure to 12 h of sunlight relative to dark controls.

	$a_{CDOM,320}$ [a]	S_R [b]	FI [c]	Peak A	Peak C	Peak T
%Δ	-9.5 (*0.2*)	17.9 (*0.3*)	-12.9 (*0.3*)	-11.2 (*0.6*)	-26.0 (*0.3*)	5 (*2*)

[a] $a_{CDOM,320}$ indicates absorption coefficient of CDOM at 320 nm
[b] S_R indicates slope ratio
[c] FI indicates fluorescence index

FIGURES

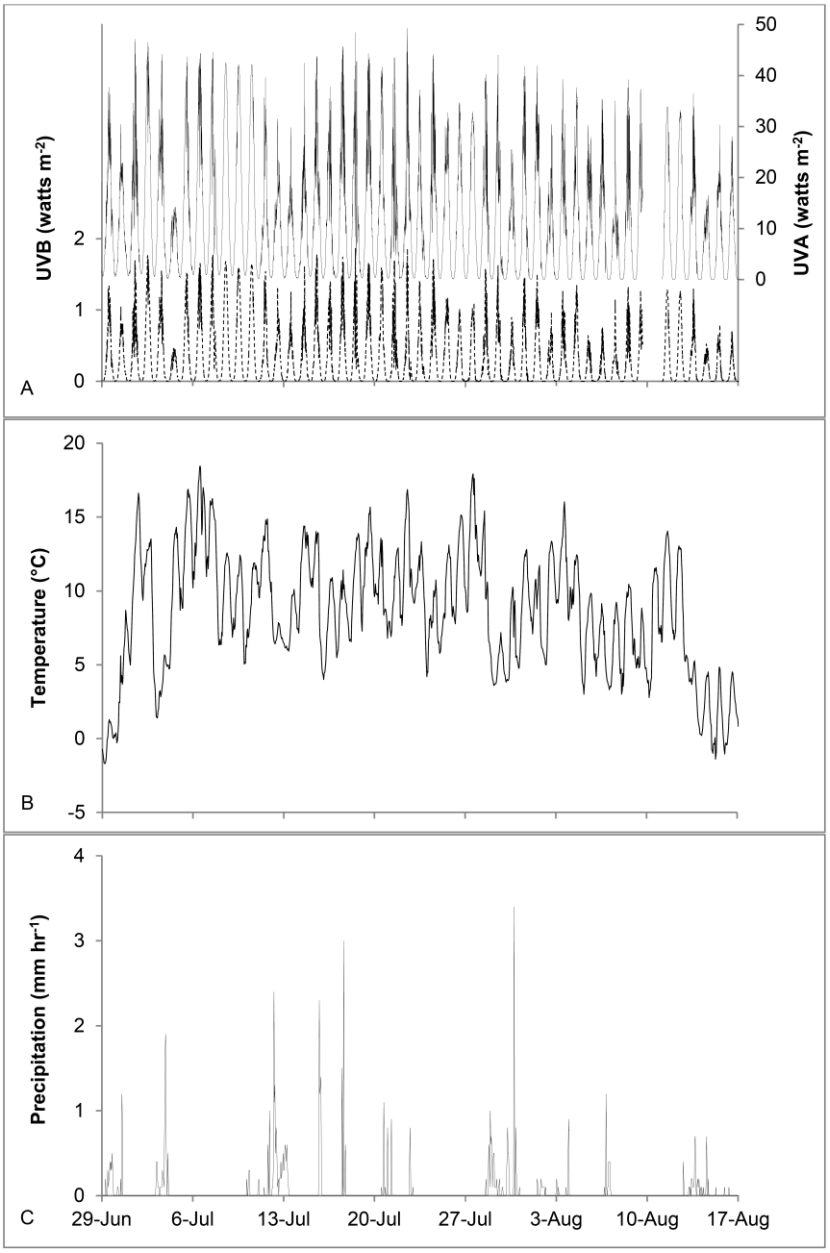

Figure 1.1. Weather variables were measured at Imnavait Creek and Toolik Field Station (TFS). Solar radiation measured at TFS exhibited diel fluctuations in both the UVB (dashed line) and UVA (solid line) (A). Air temperature at Imnavait Creek during the study period exhibited diel fluctuations and the average air temperature during the study period was 8.7 °C (B). The 2011 summer was overall dry with a few small precipitation events and a total of 7.4 cm of precipitation at Imnavait Creek during the study period (C).

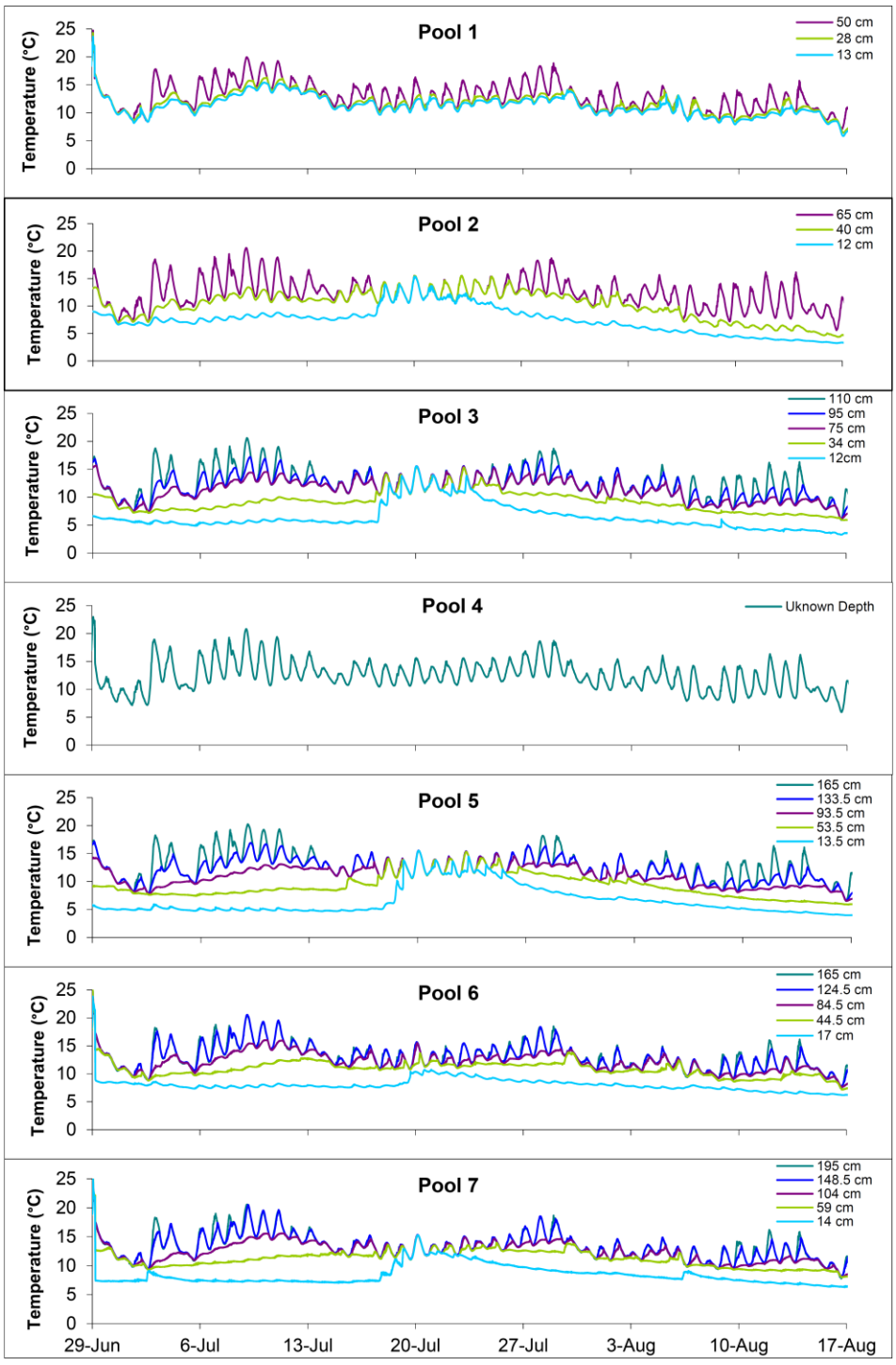

Figure 1.2. Temperature at depths measured from the bottom of the pool. Pools 2, 3, 5, 6, and 7 were stratified for most of the summer; they were mixed briefly following a storm on 17 July 2011 and re-stratified within four or five days. Pool 1 mixed every night. The shallow depth of pool 4 (0.2 m) likely contributed to it never stratifying.

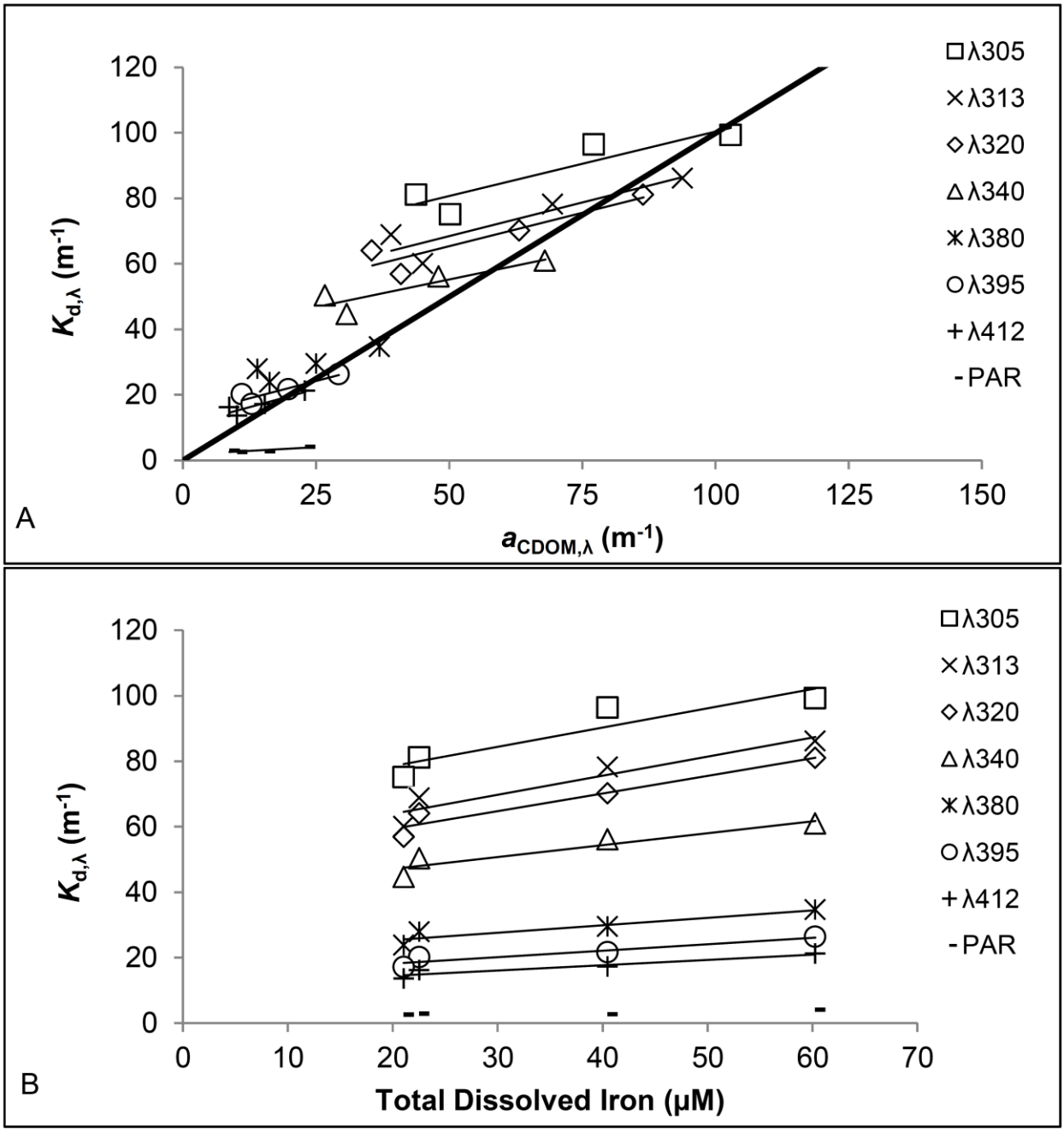

Figure 1.3. The light attenuation coefficients ($K_{d,\lambda}$) were positively correlated with both (A) CDOM absorption coefficients ($a_{CDOM,\lambda}$) shown with a 1:1 line (thick solid line) and (B) concentrations of total dissolved iron in pool waters on 27 June, 2011. Linear regressions between $K_{d,\lambda}$ and both $a_{CDOM,\lambda}$ and total dissolved iron are shown (thin solid lines). $K_{d,\lambda}$ was less than $a_{CDOM,\lambda}$ in each pool except pool 2 (i.e., points fall above the 1:1 line).

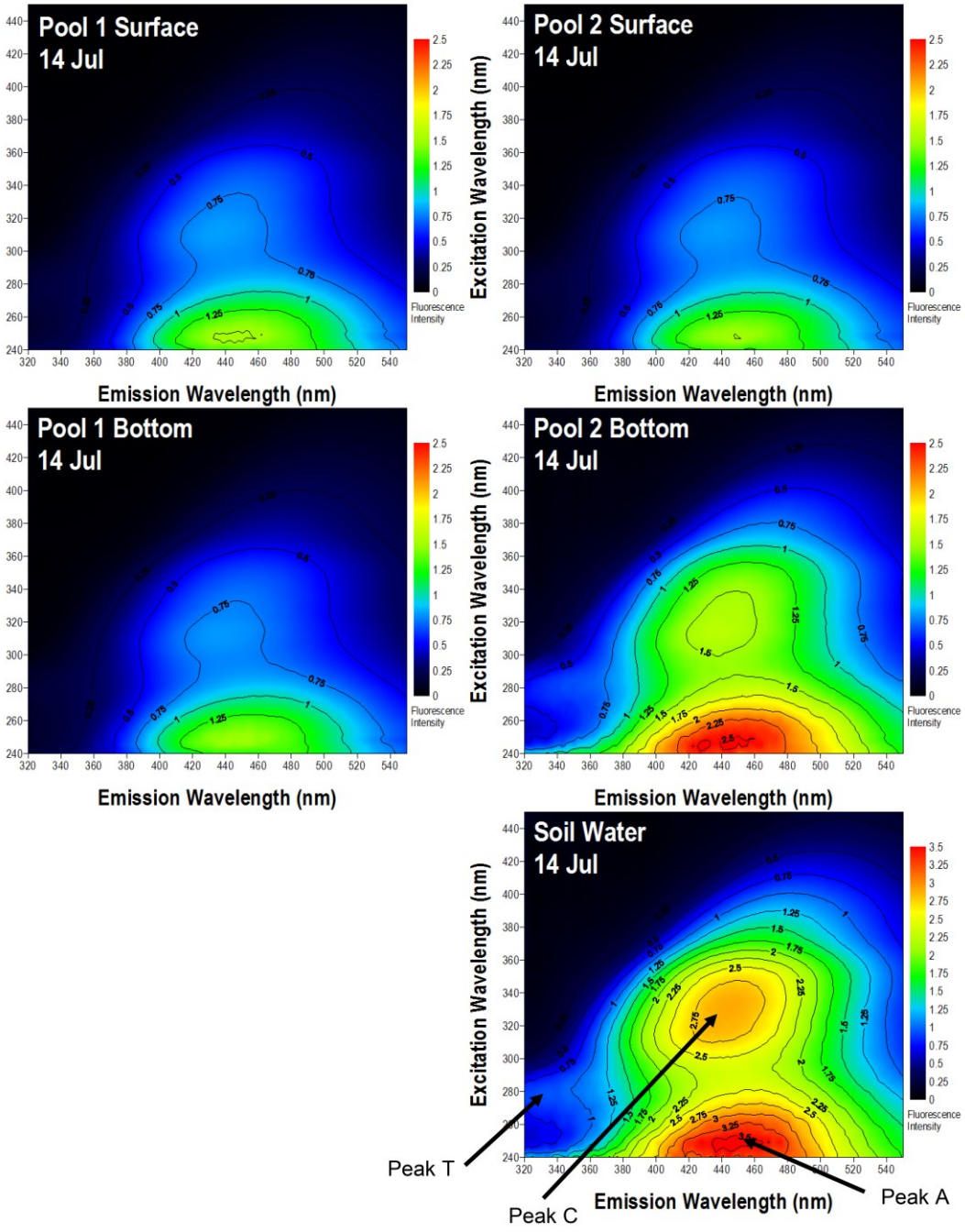

Figure 1.4. Representative EEMs of surface and bottom waters of a mixed (pool 1) and unmixed (pool 2) pool in Imnavait Creek and soil water feeding into Imnavait Creek from 14 July, 2011. The three characteristic FDOM peak regions (A, C, and T) are indicated on the soil water EEM. FDOM peak positions and intensity are similar in soil water and stratified bottom water. Likewise, the FDOM peak positions and intensity of surface water and mixed bottom water are also similar.

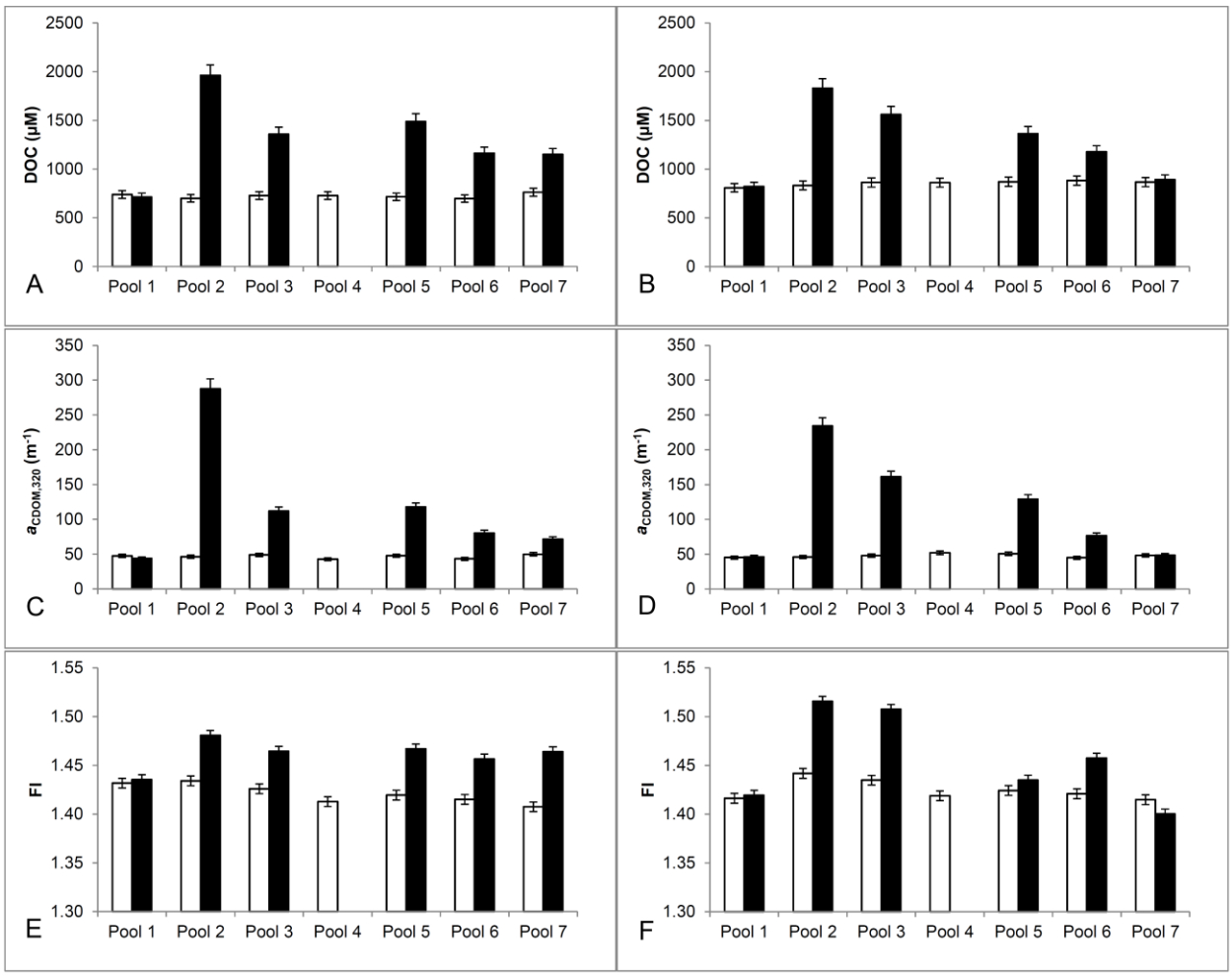

Figure 1.5. DOM quantity was greater and more variable in quality in the bottom waters (shaded bars) of stratified Imnavait Creek pools compared to the surface waters (open bars). The quantity of DOC was greater in the bottom waters of the stratified pools on 14 July, 2011 (A) and again on 4 August, 2011 (B), following re-stratification after a storm-induced mixing event. The absorption coefficient of DOM at 320 nm ($a_{CDOM,320}$) was consistently higher in the bottom waters of all stratified pools on both 14 July, 2011 (C) and 4 August, 2011 (D). Similarly, the fluorescence index (FI) of the bottom waters was greater than the surface waters in the stratified pools on both 14 July, 2011 (E) and 4 August, 2011 (F). Pool 7 does not exhibit the same recovery to pre-storm differences in chemistry as the other stratified pools. Pool 1 was mixed throughout the summer and did not show differences in surface and bottom values. Error bars are of instrumental error.

CHAPTER TWO

Aqualog fluorometer for FDOM analysis: evaluation, optimization, and comparison to a conventional fluorometer

I evaluated the analysis of the fluorescent fraction of dissolved organic matter (FDOM) using an Aqualog spectrofluorometer, a new instrument optimized for FDOM analysis. Because the effects of a spectrofluorometer on FDOM spectra can be significant, the ability to relate FDOM data collected on the new Aqualog to data collected on other instruments is unknown, thus constraining long-term monitoring studies incorporating FDOM analysis. To address this knowledge gap, I analyzed FDOM on the Aqualog across a range of dissolved organic carbon (DOC) concentrations from 100 to 0.1 mg C L^{-1}. I tested the effect of excitation and emission wavelength increments, the effect of sample dilution to evaluate the effective DOC range of the Aqualog, the range over which inner-filter effect (IFE) can be linearly corrected, and the effect of order of corrections on sample signal. I further compared the CDOM and FDOM results of forty samples analyzed using both the optimized Aqualog parameters and a separate UV-Vis coupled with a Fluoromax-4 spectrofluorometer, including two well characterized reference samples (Suwannee River fulvic acid (SRFA) and Pony Lake fulvic acid (PLFA)) and 38 filtered natural water samples ranging in DOC concentration from 2.0 to 12.9 mg C L^{-1}. For optimal analysis of CDOM and FDOM using the Aqualog I recommend dilution of samples with decadic absorption coefficient at 254 nm ($dec_{CDOM,254}$) > 60 m^{-1} and correction for instrument-specific effects and IFE consistent with current best practices in the literature. The optimal DOC range for

analysis of FDOM on the Aqualog was determined to be approximately 2 to 15 mg C L^{-1} under the parameters investigated in this study. Outside this range, there was higher standard error of mean intensities, lower signal to noise, or significant IFE. The optics and performance of different instruments means that inter-instrument variability cannot be fully removed using instrument-specific correction factors, even using NIST standard reference materials. The application of an empirical inter-instrument correction factor improved the comparison of results between instruments. However, care must be taken in interpreting the results even after inter-instrument correction.

INTRODUCTION

UV-visible absorbance and excitation-emission matrix (EEM) fluorescence spectroscopy have been used extensively to characterize dissolved organic matter (DOM), a complex and heterogeneous mixture of organic compounds produced from the breakdown of plants and microbial organic matter. Absorbance spectra of DOM typically exhibit a smooth exponential decay with increasing wavelength of light (Stedmon and Markager, 2001). Fluorescence signals of DOM tend to be broad and featureless emission curves. As DOM contains many fluorophores (emitting moiety) the emission spectra are collected as a function of excitation energies. These EEMs show a surface of wavelength-specific emission intensities plotted over a range of excitation wavelengths. Excitation and emission peak maxima (wavelength and intensity) in an EEM depend on the source of DOM (McKnight et al., 2001), whether EEM collection followed established protocols, and the instrument used for analysis (Cory et al., 2010).

Peak maxima in EEMs depend on the DOM source because the source determines the concentration and chemical composition of the fluorescent DOM (FDOM). For

example, waters receiving large inputs of humic material from terrestrial sources would be expected to have high fluorescence intensity in the peak regions associated with terrestrial humic material whereas waters with microbial inputs would be expected to contain greater concentrations of microbially-produced fluorophores (Fig. 2.1).

The most important consideration for EEM analysis is correction for the self-shading or "inner-filter effect" (IFE, Miller et al., 2010). IFE is the self-shading of DOM, which results in (1) a non-constant intensity of excitation light throughout a solution as light is absorbed exponentially as it travels from the light source through a solution prior to exciting molecules and (2) re-absorption of the emitted light as it travels from the source through a solution to the detector. The established correction for the IFE is based on the absorbance of the sample at each excitation and emission wavelength pair (ex/em):

$$\text{corrected emission intensity}_{ex/em} = \frac{\text{measured emission intensity}_{ex/em}}{10^{-0.5\ \text{cm}(A_{ex} + A_{em})}} \quad (1)$$

where A_{ex} and A_{em} are decadic absorbance by CDOM at the excitation and emission wavelength, respectively, with units of cm^{-1} (McKnight et al., 2001).

Miller et al. (2010) determined that IFE can be corrected up to absorbance values of 0.3 to 0.8 in a 1-cm pathlength cuvette. At higher absorbance values, corrected emission intensity no longer increases linearly with absorbance suggesting that IFE can't be removed from these optically thick waters.

The effect of instrument bias on fluorescence sample analysis is due to the non-uniform response of each part of a spectrofluorometer across the range of wavelengths used (Lakowicz, 2006). For example, the xenon-arc lamp used as a light source does not have constant emission output over its excitation range of approximately 230 to 600 nm and the wavelength dependent performance of gratings and emission detectors also affect

the emission signal non-uniformly. Therefore, correction of instrument-specific biases is necessary to minimize their effect on the DOM fluorescence signal (Cory et al., 2010).

Procedures for correcting EEMs for instrument specific response have been applied in many studies (e.g., Coble et al., 1993; Cory et al., 2010; DeRose et al., 2007; Holbrook et al., 2006; Miller et al., 2010). Cory et al. (2010) compared the results of instrument-specific corrections from the same samples run on three different spectrofluorometers. The correction factors improved comparability of spectra between instruments, but did not result in 100 % overlap in peak positions or emission intensities.

Thus, work to date suggests that instrument bias cannot be removed from sample signal by instrument-specific correction factors alone (Cory et al., 2010). This means that long-term data sets collected with multiple instruments must characterize and account for the effects of instrument bias. For example, SanClements et al. (2012) used analysis of FDOM to characterize and understand decadal trends in DOC concentrations. They found that the chemical signature of FDOM had changed along with DOC concentrations and used the FDOM results to support their hypothesis that changes in acid deposition had resulted in greater terrestrial inputs to surface waters due to higher solubility of soil organic matter (SanClements et al., 2012). However, the main FDOM measurement used was fluorescence index (FI) and while relative patterns of FI within a set of samples remain consistent regardless of the instrument used, the magnitude of specific samples can vary significantly between instruments (Cory et al., 2010) limiting the ability to compare datasets collected with multiple instruments.

SanClements et al. (2012) used archived samples all run on a single instrument, and was thus free from the effects of instrument bias, but studies wishing to analyze

longer term FDOM trends in a similar manner using data collected over time with multiple instruments will have to evaluate instrument specific response. These studies that rely on data collected with multiple instruments, which will occur as instrument technology continues to improve, will run into issues of instrument effects impeding the interpretation of their data. Thus, if we want to use FDOM to understand changes in any system over time due to climate or land use change, we need to understand the effect of the instrument on FDOM signals. This problem is confounded because instruments change and improve over time, and because instrument manufacturers rarely control for every variation in output or behavior of machines from one version to the next. Here I summarize the effects of instrument on FDOM signals, and demonstrate our approach to characterizing and correcting for the effect of instrument bias.

The Aqualog (Horiba; Edison, NJ) has recently been introduced as a spectrofluorometer optimized to characterize FDOM in natural waters. It includes both an absorbance detector and fluorescence detector and matching bandpass for both spectra designed specifically to minimize the IFE from natural water samples. The Aqualog also has a double grating excitation monochromator to minimize the influence of stray light thereby minimizing the effects of unwanted wavelengths of light, scattering, and emission measurement interference (Lakowicz, 2006). The goal of the new Aqualog was an instrument applicable to analysis of DOM in natural waters over a large range of DOC concentrations, from dilute seawater where the ratio of signal to noise is an issue to freshwater samples where correcting for the IFE is important.

To evaluate the analysis of DOM samples using the Aqualog I tested samples of Suwannee River fulvic acid (SRFA) across a range of concentrations from 100 to 0.1 mg

C L^{-1}. I tested the effect of excitation and emission wavelength increments, the effect of sample dilution to evaluate the effective DOC range of the Aqualog, the range over which IFE can be linearly corrected, and the effect of order of corrections on sample signal.

I compared the optimized Aqualog CDOM and FDOM results to CDOM and FDOM results collected on a "conventional" set up, in this case an Ocean Optics UV-Vis coupled with a Fluoromax-4 spectrofluorometer. I analyzed forty samples on each system, including two well characterized reference samples (SRFA and Pony Lake fulvic acid (PLFA)) and 38 filtered natural water samples ranging in DOC concentration from 2.0 to 12.9 mg C L^{-1}. I compared uncorrected and corrected EEMs between each system on the dataset of 40 samples to evaluate how well instrument-specific corrections minimized instrument bias. I also developed two average empirical correction factors between the two systems using the dataset of 40 samples and evaluated the ability of the empirical correction factors to minimize instrument-specific bias.

METHODS

Optimizing analysis of CDOM and FDOM using the Aqualog

Solution preparation

A stock solution of 200 mg Suwannee River Fulvic Acid (SRFA) L^{-1} was prepared from an International Humic Substance Society standard (I 1S101F) in laboratory-grade deionized (DI) water (Dracor, Inc.; Durham, NC). The solution was stirred for 24 hours at room temperature, adjusted to pH 7.19 with sodium hydroxide, and filtered through pre-combusted Whatman GF/F glass fiber filters (Whatman; Clifton, NJ). The stock solution was diluted with DI to 16 concentrations ranging from approximately

0.1 to 100 mg C L^{-1}. The final pH of the most concentrated sample analyzed was 6.78 and the final pH of the most dilute sample was 6.32.

DOM characterization

UV-Vis absorbance spectra of CDOM were collected in triplicate at two different increments (3 and 5 nm) using 1-cm path length quartz cuvettes measured against DI blanks using an Aqualog silicon photodiode detector (Horiba; Edison, NJ). Spectra were interpolated to 1 nm increments using Matlab (version 7.7). The spectral slope ratio (S_R) was calculated from the absorbance spectrum of each sample as the ratio of the slope from 275 to 295 nm to the slope from 350 to 400 nm following Helms et al. (2008). Naperian CDOM absorption coefficients ($a_{CDOM,\lambda}$) were calculated as follows:

$$a_{CDOM,\lambda} = \frac{A_\lambda}{l} 2.303 \qquad (2)$$

where A is the absorbance reading at wavelength λ and l is the pathlength in meters. Likewise, decadic CDOM absorption coefficients, $dec_{CDOM,\lambda}$, were calculated as follows:

$$dec_{CDOM,\lambda} = \frac{A_\lambda}{l} \qquad (3)$$

Excitation-emission matrices (EEMs) were measured on the Aqualog with a charge-coupled device (CCD) detector (Horiba). Briefly, triplicate EEMs were collected from each sample over excitation and emission ranges of 240 to 600 nm at two different increment pairs for a total of six EEMs per concentration of SRFA. The two excitation/emission increment pairs were 3/3.28 and 5/1.64 nm/nm. These increments were selected based on the Horiba recommendation that excitation and emission increments match as closely as possible, and to closely match increments used in

previous studies on older instruments (e.g., 5/2 nm/nm on a Fluoromax-3; Cory et al., 2010), respectively. All samples were analyzed with medium gain. Integration time ranged from 0.3 to 4 seconds and was held constant at each concentration of SRFA (i.e., the same integration time was used for all six EEMs collected at each concentration). Fresh sample was placed in the 1-cm quartz cuvette for each concentration of SRFA. Aqualog software corrects all EEMs for dark offset, instrument-specific excitation and emission correction, blank subtraction, and IFE correction. The Chapman Conference on Organic Matter Fluorescence (2008) reached consensus on the order of EEM correction as: IFE, instrument-specific excitation and emission correction factors, and blank subtraction. Thus, corrected sample EEMs exported from the Aqualog software were uncorrected for instrument-specific excitation and emission correction spectra followed by correction for IFE and instrument-specific excitation and emission corrections in Matlab (version 7.7) following Cory et al. (2010) using manufacturer provided instrument-specific excitation and emission correction spectra (Horiba Scientific). Similarly analyzed blank EEMs, of DI water free of detectable fluorescence emission, were subtracted from sample EEMs to minimize the influence of water Raman peaks. Lastly, intensities of corrected sample EEMs were converted to Raman units (RU; Stedmon and Bro, 2008). The fluorescence index (FI; McKnight et al., 2001) was calculated from each corrected EEM as the ratio of emission intensity at 470 nm over the emission intensity at 520 nm at an excitation wavelength of 370 nm (Cory et al., 2010). EEMs were interpolated to 1 nm increments. Emission intensity at peaks A, C, and T, which represent humic and protein fluorescent moieties, was evaluated at

excitation/emission pairs 250/450, 350/450, 275/340 nm/nm, respectively, in RU (Coble et al., 1990).

Comparison of Aqualog to Fluoromax-4

Sample analysis

Forty samples (including SRFA, PLFA, and 38 natural water samples) spanning a range of DOC, CDOM, and FDOM concentrations were analyzed on both the Aqualog and Fluoromax-4. All samples were filtered through pre-combusted GF/F glass fiber filters (Whatman) and stored at 4 °C in the dark until analysis. The analyses on the two instruments occurred within minutes of each other on identical sample aliquots.

CDOM was analyzed in three ways, depending on the concentration of CDOM in a sample. All samples were analyzed in quartz cuvettes. The analysis of samples with CDOM greater than approximately $dec_{254,CDOM}$ of 10 m^{-1} consisted of analysis using the Aqualog built-in silicon photodiode detector and analysis using an Ocean Optics spectrophotometer (Ocean Optics, Inc.; Dunedin, FL) both using a 1-cm pathlength cuvette. CDOM data from the Aqualog detector was used with FDOM data collected using the Aqualog and CDOM data from Ocean Optics spectrophotometer was used with FDOM data collected using the Fluoromax-4. Additionally, samples with low concentrations of CDOM ($dec_{254,CDOM}$ less than approximately 10 m^{-1}) were analyzed with a 5-cm pathlength cuvette using a Hewlett Packard spectrophotometer (HP 8452 Diode Array Spectrophotometer). In the case of low CDOM samples, the same UV-Vis spectrum was used with FDOM data from both the Aqualog and Fluoromax-4. Sample absorption was measured against laboratory-grade deionized (DI) water blanks.

Analysis of FDOM using the Aqualog was similar to the description above in DOM Characterization. However, an excitation increment of 5 nm was used for all samples and each sample was only analyzed one time following the optimal integration time as determined by the fluorescent intensity with a 0.1 second integration time and "optimum integration time" table in the Aqualog manual. Samples were analyzed with an emission increment of 1.64 nm unless $dec_{CDOM,254}$ was less than approximately 10 m^{-1} in which case an emission increment of 3.28 nm was used.

Analysis of FDOM using the Fluoromax-4 was done with excitation/emission increments of 5/2 nm/nm and a 0.1 second integration time following Cory et al. (2010).

EEMs from both instruments were corrected for IFE and for instrument-specific excitation and emission corrections in Matlab (version 7.7) following Cory et al. (2010). Aqualog EEMs were corrected using manufacturer-provided correction factors including an emission correction factor generated using NIST reference materials. Fluoromax-4 EEMs were corrected two different ways: (1) using a user-generated rhodamine excitation correction factor ($excorr_{FM\text{-}rhod}$) and the original Horiba-provided emission correction factor ($emcorr_{FM\text{-}OrigHoriba}$) and (2) an excitation correction factor created with a Horiba excitation correction kit ($excorr_{FM\text{-}HoribaKit}$; Excitation Correction Factor Kit, F-3028, Horiba) and an emission correction factor generated using Horiba's NIST standard reference materials ($emcorr_{FM\text{-}SRM}$).

Corrected EEMs from the Aqualog were interpolated to the same range as was used to collect EEMs on the Fluoromax-4 (i.e., ex/em 5/2 nm/nm) for all comparisons and analyses.

Inter-instrument correction factor

Two empirical inter-instrument correction factors were developed from the forty samples analyzed on both the Fluoromax-4 and Aqualog. The correction factors were made by averaging the ratio of the fluorescence intensity of each sample collected with the Fluoromax-4 and Aqualog at each ex/em pair. Outliers due to stray scattering peaks at specific ex/em pairs were excluded from the correction factor. The difference between the two correction factors is that one was made using Fluoromax-4 EEMs corrected using $excorr_{FM\text{-}rhod}$ and $emcorr_{FM\text{-}OrigHoriba}$ and the other using $excorr_{FM\text{-}HoribaKit}$ and $emcorr_{FM\text{-}SRM}$.

These correction factors were evaluated by comparing the results (e.g., FI, fluorescence intensity at peaks A, C, and T, and ratios of peaks C and A (C/A) and peaks T and A (T/A)) of corrected EEMs collected with the Fluoromax-4 with and without the additional correction for the inter-instrument variation to corrected EEMs collected with the Aqualog.

RESULTS

Absorbance

There was substantial overlap between absorbance spectra collected at 3 and 5 nm increments (e.g., Fig. 2.2). The standard error of replicate (n = 3) absorption coefficients ($a_{CDOM,\lambda}$) measured using the same settings ranged from < 0.01 to 1.08 m^{-1} depending on wavelength and concentration of the sample. The difference between average (n = 3) $a_{CDOM,\lambda}$ measured at 3 and 5 nm increments ranged from < 0.01 to 0.57 m^{-1} depending on wavelength and concentration of the sample. Thus, the range of variability between replicates and between samples measured with different increments was of a similar scale.

Absorption coefficients of CDOM ($a_{CDOM,\lambda}$ and $dec_{CDOM,\lambda}$) were highly correlated with the concentration of DOC (e.g., Fig. 2.3; $r^2 \geq 0.99$ at all wavelengths).

Excitation and emission increments

There was no significant difference between corrected emission fluorescence intensities collected with excitation/emission increments of 3/3.28 and 5/1.64 nm/nm at peaks A, C, or T (Fig. 2.4; t-test, $p > 0.05$).

Inner-filter effects

Uncorrected fluorescence intensities of SRFA exhibited strong IFE shown by a nonlinear increase in emission intensity at peaks A, C, and T as a function of increasing CDOM concentration (decadic absorption coefficient at 254 nm; $dec_{CDOM,254}$) (Fig. 2.5). This is because emission intensity should increase linearly with increasing sample absorbance in the absence of an IFE (Lakowicz, 2006). The IFE has a greater effect on peak A and T emission compared to peak C (Fig. 2.5). The choice of excitation/emission increments (3/3.28 vs. 5/1.64 nm/nm) had no detectable influence on the IFE (Fig. 2.5).

IFE corrections improved the linear emission at peaks A, C, and T for samples with $dec_{CDOM,254} \leq$ approximately 60 m^{-1} (Fig. 2.4). Above this concentration of CDOM the fluorescence intensity of peaks A and T deviated from the linear trend; peak C remained linear at higher concentrations of CDOM. There was no significant difference between the fluorescence intensity of EEMs collected with excitation/emission increments of 5/1.64 nm/nm (black squares) compared to EEMs collected with excitation/emission increments of 3/3.28 nm/nm (hollow diamonds). This result is consistent with Miller et al. (2010) who report that IFE could be linearly corrected in samples with $dec_{CDOM,254} \leq 0.3$ to 0.8 (unitless, collected in a 1-cm pathlength cuvette).

Thus, the data suggest that independent of instrument, there is a threshold at which samples must be diluted prior to EEM analysis for IFE to be correctable.

Order of corrections

The order of corrections did affect the corrected EEM (Fig. 2.6). The order of corrections used in the Aqualog software resulted in negative Rayleigh and Raman scatter peaks of greater magnitude than the scatter peaks in EEMs corrected following the Chapman Conference order (Fig. 2.6).

Effect of concentration

S_R and FI are both intrinsic properties of DOM that should remain constant regardless of concentration assuming instrument bias is removed from sample signal. However, I found that at the low concentrations investigated in this study (0.1 to 1 mg C L^{-1}) the Aqualog measurements of S_R and FI deviated from the expected constant results observed at the mid-ranges of DOC (2 to 15 mg C L^{-1}) (Fig. 2.7). Additionally, at the low concentrations investigated in this study, high variability was observed in S_R and FI as quantified by the standard error (SE) for these dilute samples (Fig. 2.7), potentially due to decreased signal to noise. At high concentrations (20 to 100 mg C L^{-1}), there was likewise a deviation from the less variable measurements at mid-concentrations, likely due to IFE beyond the linear range of correction. These deviations at low and high concentrations from the mean values at mid-range DOC concentrations were observed independently of the choice of excitation/emission increments tested (Fig. 2.7).

Minimizing instrument bias

Instrument-specific correction factors

Correcting samples with the instrument-specific correction factors resulted in poor agreement between values measured on both instruments as shown by the large differences between the data points and 1:1 lines (Fig. 2.8 and 2.9). If the instrument-specific correction factors were sufficient to remove instrument bias we would expect the data points to fall on a 1:1 line, but the 95 percent confidence intervals of the slopes of Aqualog versus Fluoromax-4 data corrected with instrument-specific factors did not encompass 1 for any value measured (i.e., FI and peak intensities). For example, the difference between the corrected FI values of a sample measured on both instrument ranged from less than 0.01 to 0.16 regardless of which Fluoromax-4 correction factors were used, which is greater than replicate error of 0.01 to 0.03 for FI measured on a single instrument (Fig. 2.8). There was poor agreement between corrected peak fluorescence intensities measured on the two instruments regardless of the instrument-specific correction factors used, but the difference was greater when the Fluoromax-4 EEMs were corrected with $excorr_{FM\text{-}HoribaKit}$ and $emcorr_{FM\text{-}SRM}$. The difference in corrected peak intensities ranged from 0.01 to 2.91 RU, representing 22 to 131 absolute percent difference relative to the corrected Aqualog value when the Fluoromax-4 EEMs were corrected with $excorr_{FM\text{-}HoribaKit}$ and $emcorr_{FM\text{-}SRM}$ (Fig. 2.9). The difference in corrected peak intensities of Fluoromax-4 EEMs corrected with $excorr_{FM\text{-}rhod}$ and $emcorr_{FM\text{-}OrigHoriba}$ ranged from less than 0.01 to 1.09 RU, representing 19 to 37 absolute percent difference relative to the corrected Aqualog values (Fig. 2.9). Typical replicate

variability for fluorescence intensity at peaks A, C, and T measured on a single instrument ranges from 0.01 to 0.07 RU.

The linear relationship between the ratios of peaks C/A and T/A measured on the two instruments were closer to the expected slope of 1 when the Fluoromax-4 EEMs were corrected with $excorr_{FM\text{-}rhod}$ and $emcorr_{FM\text{-}OrigHoriba}$ than when corrected with $excorr_{FM\text{-}HoribaKit}$ and $emcorr_{FM\text{-}SRM}$ (Fig. 2.10). For example, for the ratio of C/A measured on the two instruments the 95 percent confidence interval of the slope was 0.26 to 0.34 when using $excorr_{FM\text{-}HoribaKit}$ and $emcorr_{FM\text{-}SRM}$ and 0.62 to 0.81 when using $excorr_{FM\text{-}rhod}$ and $emcorr_{FM\text{-}OrigHoriba}$. Likewise, the 95 percent confidence intervals of the slope of the T/A ratio measured on the two instruments was 1.16 to 1.21 when using $excorr_{FM\text{-}HoribaKit}$ and $emcorr_{FM\text{-}SRM}$ and 1.00 to 1.04 when using $excorr_{FM\text{-}rhod}$ and $emcorr_{FM\text{-}OrigHoriba}$. The slope of the linear fit of the T/A data on the two instruments was closer to 1 than the fit of the C/A data (Fig. 2.10), consistent with the better fit at peaks T and A compared to peak C (Fig. 2.9).

Empirical inter-instrument correction factors

Empirically-derived inter-instrument correction factors did not improve the agreement between FI measured on the two instruments (Fig. 2.8). As shown in Fig. 2.8, a plot of sample FI analyzed on each instrument fell far from the expected 1:1 line (i.e., the same FI value should be measured on different instruments for a given sample if all instrument bias is removed). The difference between FI values measured on the Aqualog and Fluoromax-4 after applying an empirical correction factor still ranged from less than 0.01 to 0.16. Plotting the percent difference of the inter-instrument corrected Fluoromax-4 and Aqualog FI versus the concentration of CDOM ($a_{CDOM,320}$) revealed a systematic

bias in the results (Fig. 2.8). After correction with the empirical correction factors, samples with high CDOM concentrations had higher FI when analyzed using the Fluoromax-4 compared to when analyzed using the Aqualog, and samples with low CDOM concentrations had lower FI when analyzed using the Fluoromax-4 than when using the Aqualog.

Application of an empirically derived correction factor to already instrument-corrected EEMs greatly improved the agreement between fluorescence intensity at peaks A, C, and T (Fig. 2.9). The 95 % confidence intervals of the slopes were all closer to one, as would be expected in instrument bias was removed, for all peaks and peak ratios following application of the empirical correction factor. The greatest variability between the instruments after inter-instrument correction was observed at peak C; the difference in corrected peak C values measured on the two instruments ranged from less than 0.01 to 0.18 RU for Fluoromax-4 EEMs corrected with $excorr_{FM\text{-}rhod}$ and $emcorr_{FM\text{-}OrigHoriba}$ and the associated empirical correction factor and from less than 0.01 to 0.16 RU when corrected with $excorr_{FM\text{-}HoribaKit}$ and $emcorr_{FM\text{-}SRM}$ and the associated empirical correction factor. Similarly, the ratios of peaks C to A (C/A) and T to A (T/A) measured on the two instruments were in much better agreement following correction with an empirically-derived correction factor, regardless of which instrument-specific correction factors were used to correct the initial Fluoromax-4 EEMs (Fig. 2.10).

CONCLUSIONS AND RECOMMENDATIONS

There was no significant difference between CDOM or FDOM results from analysis with excitation/emission increments of 5/1.64 compared to 3/3.28 nm/nm. However, increasing the binning (i.e., emission increment) may increase the signal to

noise ratio at low FDOM concentrations in addition to increasing the integration time, and thus may be advisable for samples with low concentrations of FDOM.

Correcting for IFE improves linear response of FDOM emission intensity with increasing concentration of CDOM, but correction does not eliminate self-shading effects from high CDOM samples at low excitation wavelength. I recommend dilution for samples with $dec_{CDOM,254} > 60\ m^{-1}$, consistent with results from Miller et al. (2010).

The order of corrections applied to sample and blank EEMs affects the magnitude of the Rayleigh and Raman scatter peaks as well as the sign of the Rayleigh peak. I was able to reproduce the Aqualog-output corrected EEMs by correcting following the same order of corrections used by the Aqualog Horiba software. However, the order of corrections differs from the recommended practice of the scientific community and results in large differences in the apparent magnitude of scatter peaks compared to recommended practice. I suggest that any deviation from the recommended order of corrections could affect the apparent intensity of scatter peaks, and would need to be tested.

There is high variability in CDOM absorption coefficients and FDOM intensity for dilute samples (DOC < 1 mg C L^{-1}). The parameters investigated in this study were unable to improve the signal of CDOM or FDOM at low DOC concentrations. Future work will further investigate optimization for dilute samples.

Because of the effects of self-shading at high concentrations of CDOM and low signal to noise ratio at low CDOM and FDOM concentrations, the Aqualog performs best for samples within a DOC range of approximately 2 to 15 mg C L^{-1} under the parameters investigated in this study.

Instrument-specific correction factors, even using NIST standard reference materials, are not sufficient to remove instrument-specific biases. Thus, the development and application of empirical inter-instrument correction factors is necessary to compare results between instruments. However, care must be taken in interpreting the results even after inter-instrument correction. The optics and performance of different instruments means that inter-instrument variability cannot be fully removed. Thus, there are inherent biases in results such as FI at high and low concentrations of CDOM and FDOM. Agreement between peak positions and peak ratios appears to be more correctable. After inter-instrument correction, agreement between instruments appeared greatest at low and high excitation wavelengths and was lowest at mid excitation wavelengths.

FIGURES

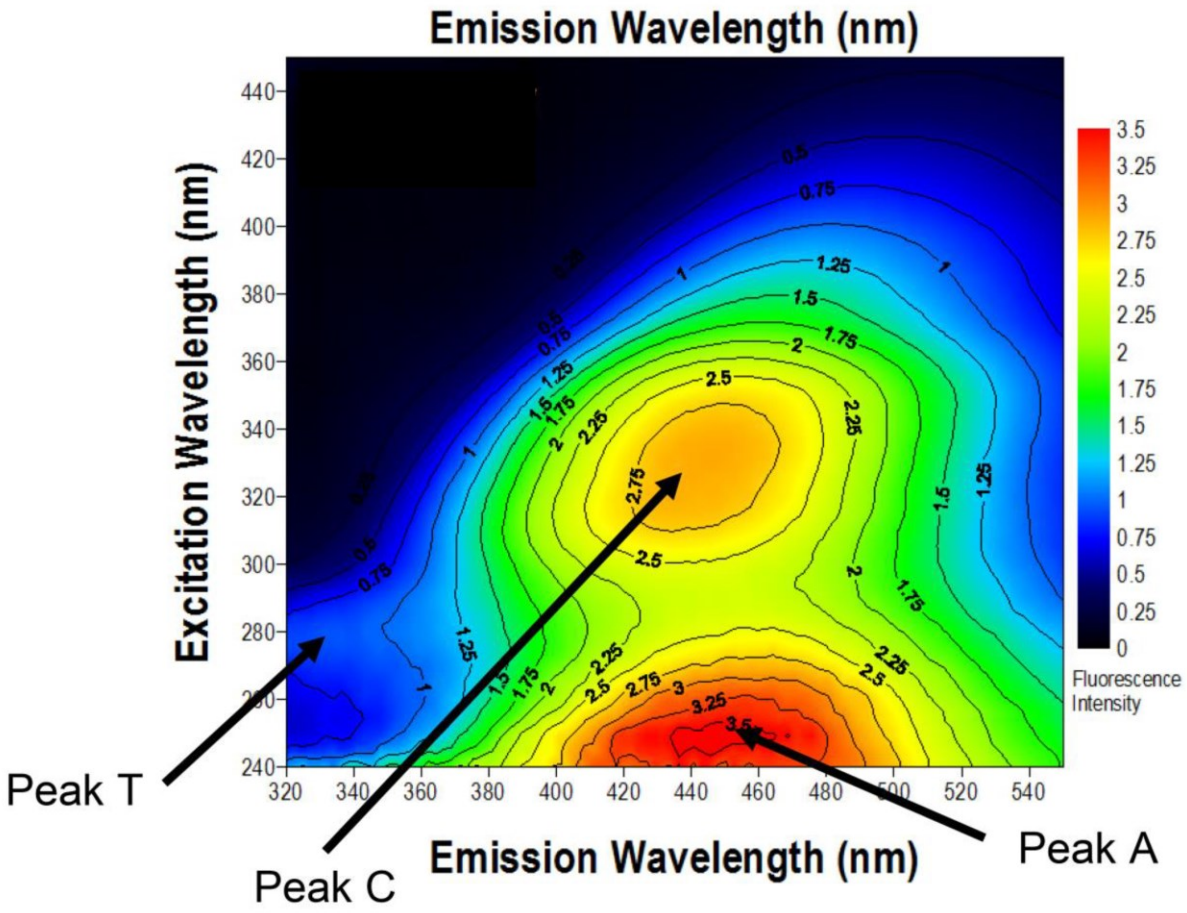

Figure 2.1. A representative EEM of DOM. The three characteristic FDOM peak regions (A, C, and T) are indicated. Peaks A and C are associated with humic material and peak T is amino acid or protein like.

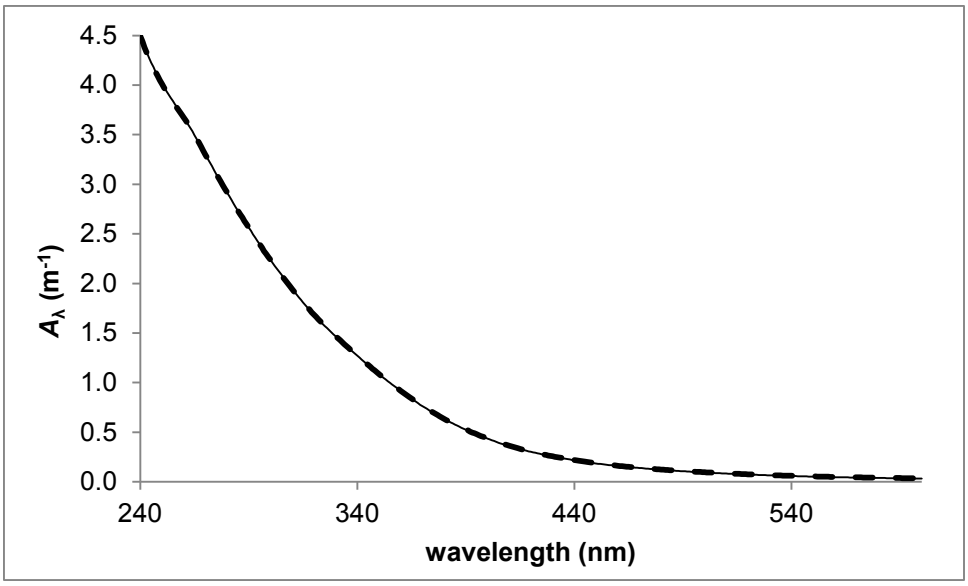

Figure 2.2. Average (n = 3) absorbance spectra of SRFA (nominal DOC = 50 mg C L^{-1}) interpolated to 1 nm increments collected at 3 nm increments (dashed line) and 5 nm increments (solid line). The spectra overlap nearly exactly at all wavelengths.

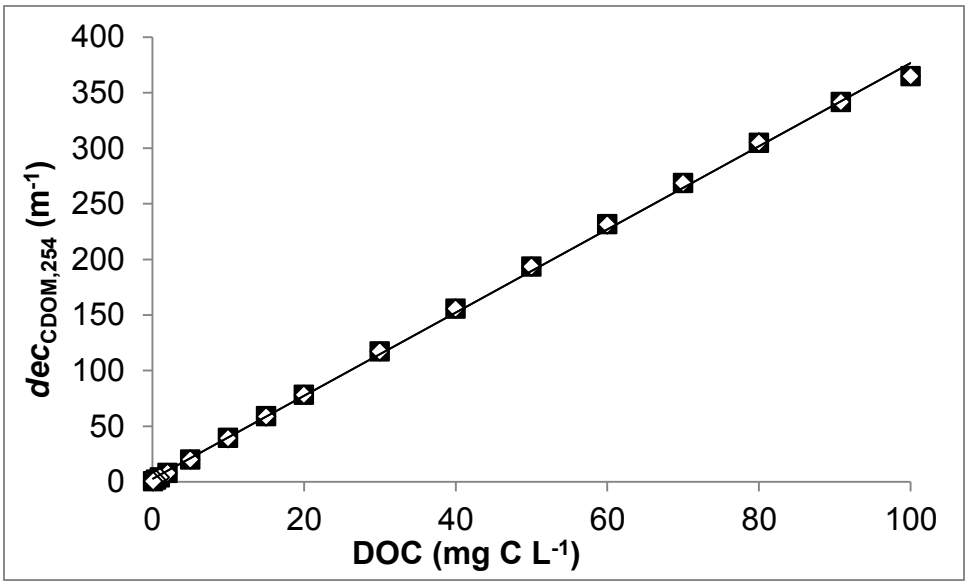

Figure 2.3. Absorption coefficients (mean ± SE) were highly correlated with DOC (e.g., decadic absorption coefficient at 254 nm; $dec_{CDOM,245}$; $r^2 \geq 0.99$). Absorbance was collected at both 5 nm (black squares) and 3 nm (hollow diamonds) increments and interpolated to 1 nm increments. Error bars smaller than the symbols are not visible.

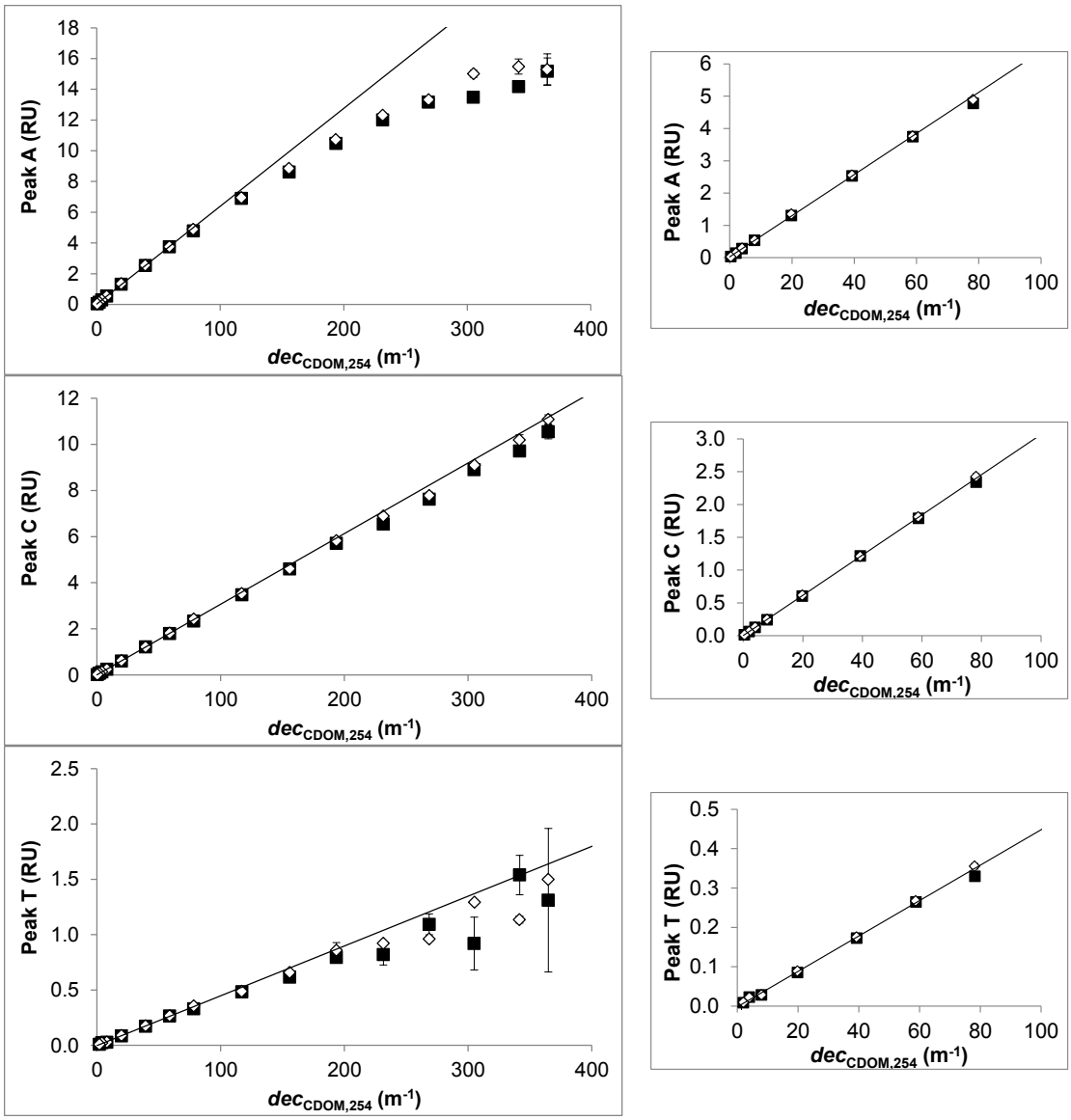

Figure 2.4. The fluorescence intensity (RU) at peaks A, C, and T (mean ± SE) collected with excitation/emission increments of 5/1.64 nm/nm (black squares) and 3/3.28 nm/nm (hollow diamonds) is plotted against CDOM concentration (decadic absorption coefficient at 254 nm; *dec* $_{CDOM,254}$) along with the linear relationship between fluorescence intensity at each peak and CDOM concentration of samples with *dec* $_{CDOM,254} \leq 60$ m^{-1}.

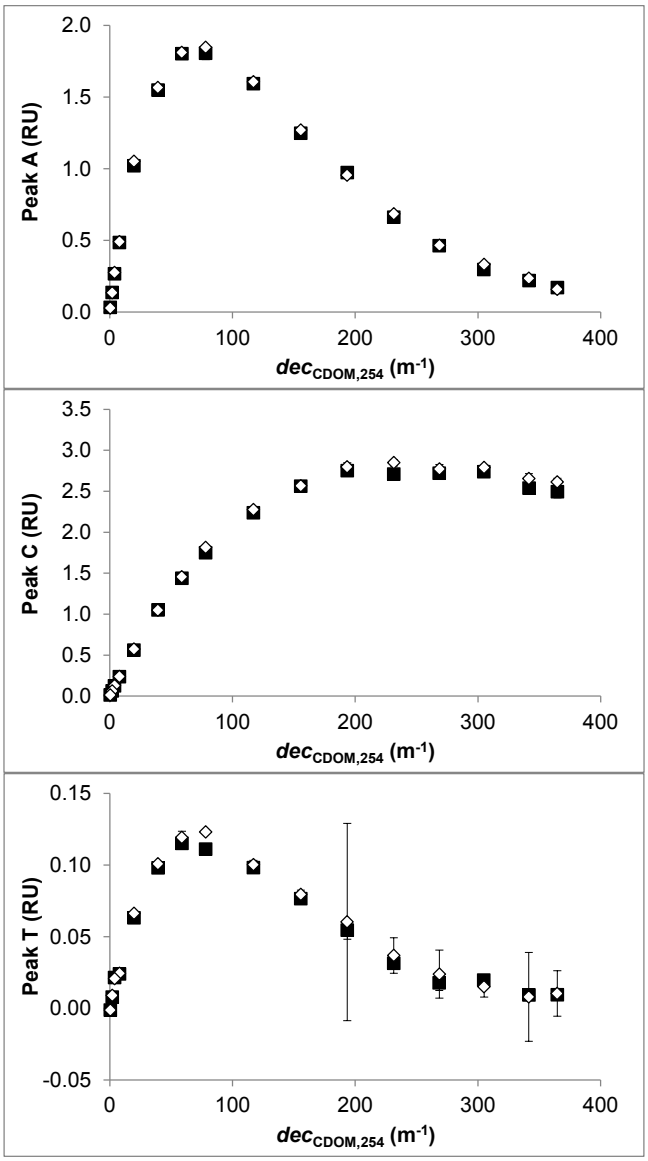

Figure 2.5. The uncorrected fluorescence intensity (RU) of peaks A, C, and T (mean ± SE) collected with excitation/emission increments of 5/1.64 nm/nm (black squares) and 3/3.28 nm/nm (hollow diamonds) are plotted against CDOM concentration (decadic absorption coefficient at 254 nm; $dec_{CDOM,254}$) all show a strongly non-linear response with increasing concentration of CDOM.

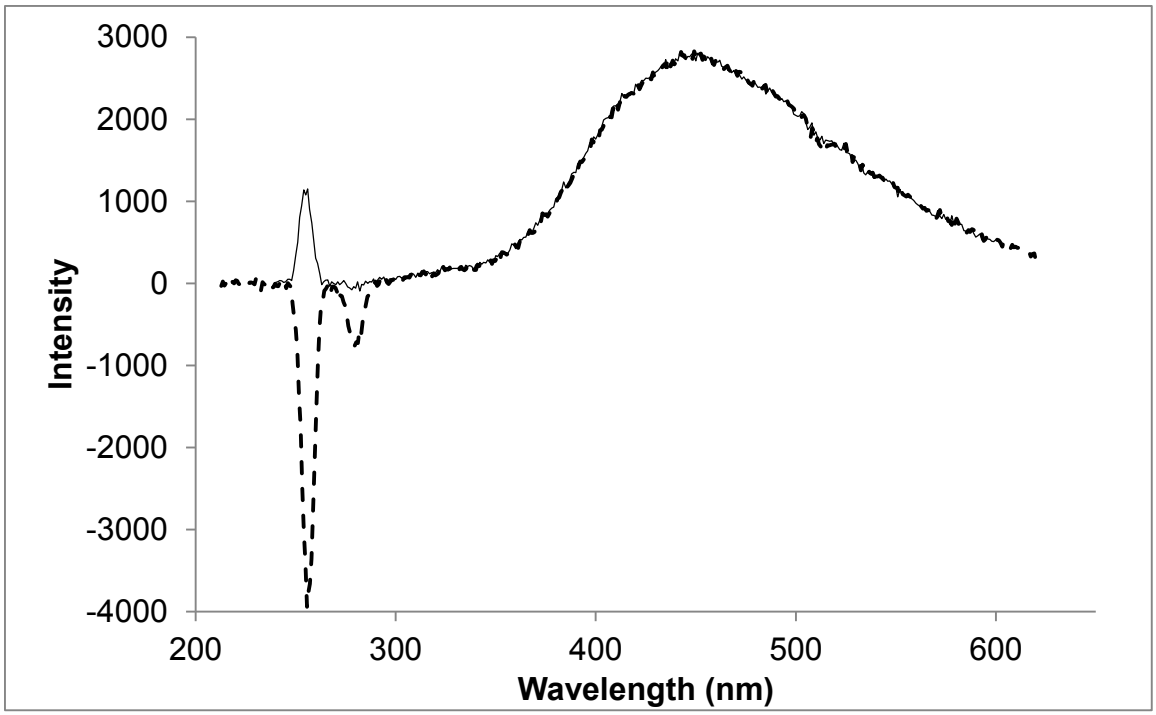

Figure 2.6. Emission spectra at excitation 255 nm of an EEM corrected following the Chapman Conference order of operations (solid line) and an EEM corrected following the Horiba Aqualog software order of operations (dashed line). Correction following the Chapman Conference order (i.e., IFE, instrument-specific excitation and emission correction, blank subtraction) resulted in smaller Rayleigh scattering and minimal influence of Raman scattering compared to EEMs corrected with the Horiba Aqualog software order of operations (i.e., instrument-specific excitation and emission correction, blank subtraction, IFE).

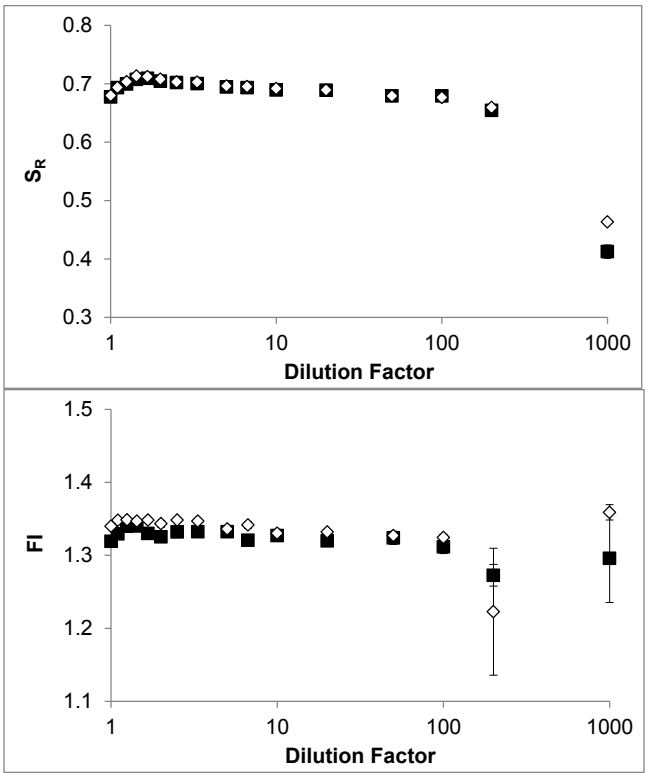

Figure 2.7. Slope ratio (S_R) and fluorescence index (FI) (mean ± SE, n = 3) of 100 mg C L^{-1} SRFA analyzed at 16 dilutions factors, 1 to 1000 (corresponding to DOC concentrations of 100 to 0.1 mg C L^{-1}), and then corrected for dilution. S_R and FI values are plotted against dilution factor (on a log scale). Samples were analyzed with excitation/emission increments of both 5/1.64 nm/nm (hollow diamonds) and 3/3.28 nm/nm (black squares).

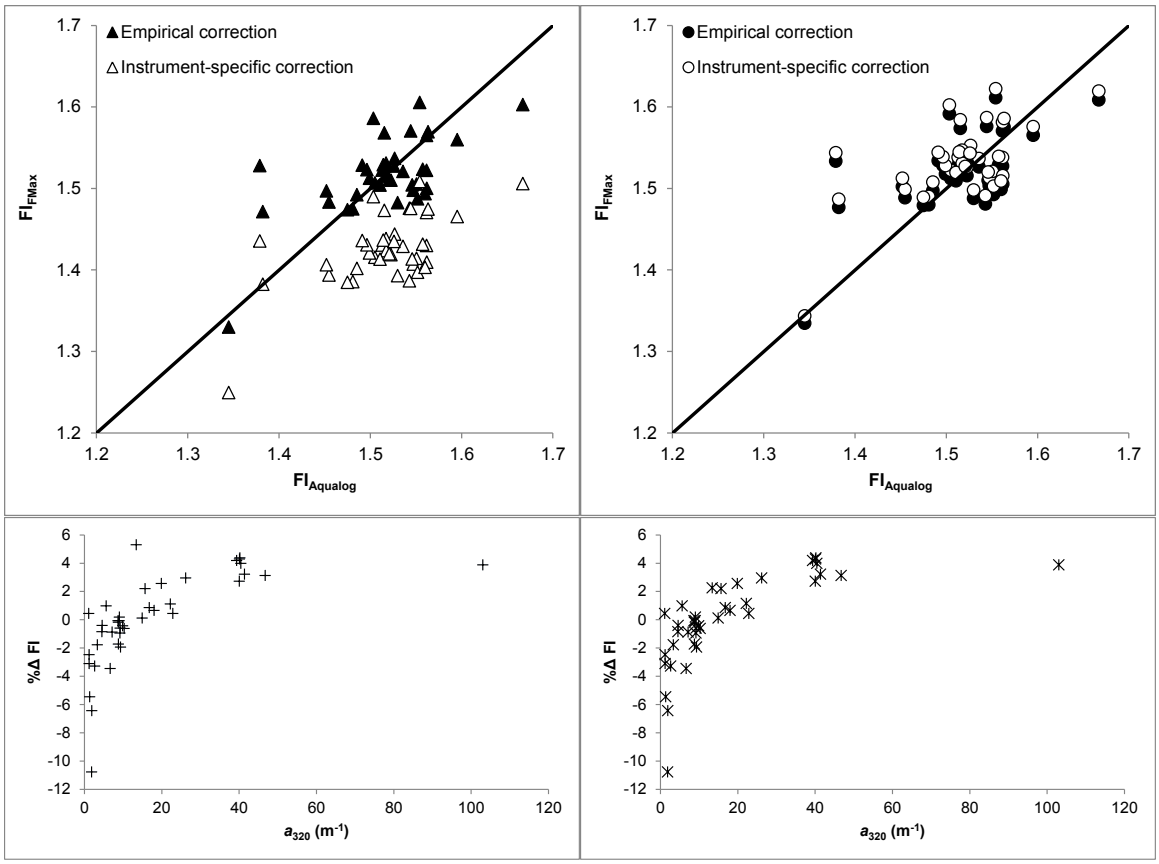

Figure 2.8. Forty samples spanning a range of DOC and CDOM concentrations were analyzed on both the Fluoromax-4 and the Aqualog and corrected following the Chapman Conference order. The paired corrected EEMs were used to develop two empirical correction factors between the Fluoromax-4 and the Aqualog: one used Fluoromax-4 EEMs corrected with $excorr_{FM\text{-}rhod}$ and $emcorr_{FM\text{-}OrigHoriba}$ and the other with $excorr_{FM\text{-}HoribaKit}$ and $emcorr_{FM\text{-}SRM}$. (A) the FI from analysis on the Aqualog plotted against FI from analysis on the Fluoromax-4 corrected using $excorr_{FM\text{-}rhod}$ and $emcorr_{FM\text{-}OrigHoriba}$ (open triangles) and the Aqualog FI versus the same corrected Fluoromax-4 further corrected with an empirically derived correction factor between the two instruments (black triangles). (B) the corrected Aqualog FI values versus the $excorr_{FM\text{-}HoribaKit}$ and $emcorr_{FM\text{-}SRM}$ corrected Fluoromax-4 FI values (open circles) and the Aqualog FI values versus the same corrected Fluoromax-4 FI values further corrected with an empirically derived correction factor between the two instruments (black circles). (C) and (D) the percent difference of the inter-instrument empirically corrected Fluoromax-4 and Aqualog FI values plotted against $a_{CDOM,320}$ revealing a systematic bias in the results.

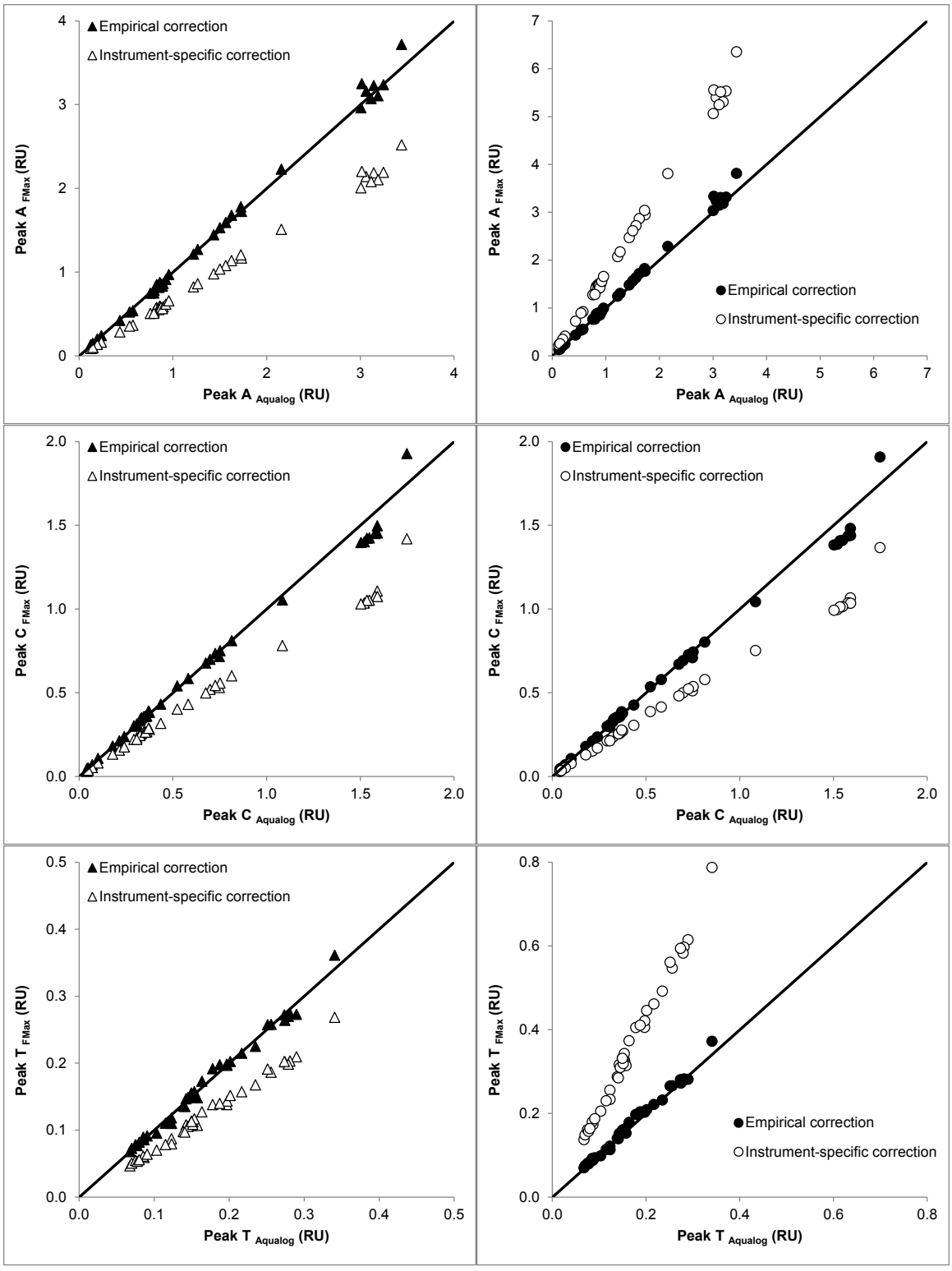

Figure 2.9. The fluorescence intensity at peaks A, C, and T as measured on the Fluoromax-4 and Aqualog plotted against each other along with a 1:1 line. Triangles are used for samples where the Fluoromax-4 data was corrected using $excorr_{FM\text{-}rhod}$ and $emcorr_{FM\text{-}OrigHoriba}$. Circles are used for samples where the Fluroomax-4 data corrected

using the $excorr_{FM\text{-}HoribaKit}$ and $emcorr_{FM\text{-}SRM}$. Open symbols represent samples corrected only with the respective instrument-specific correction factors and shaded symbols represent samples further corrected with an empirically derived inter-instrument correction factor.

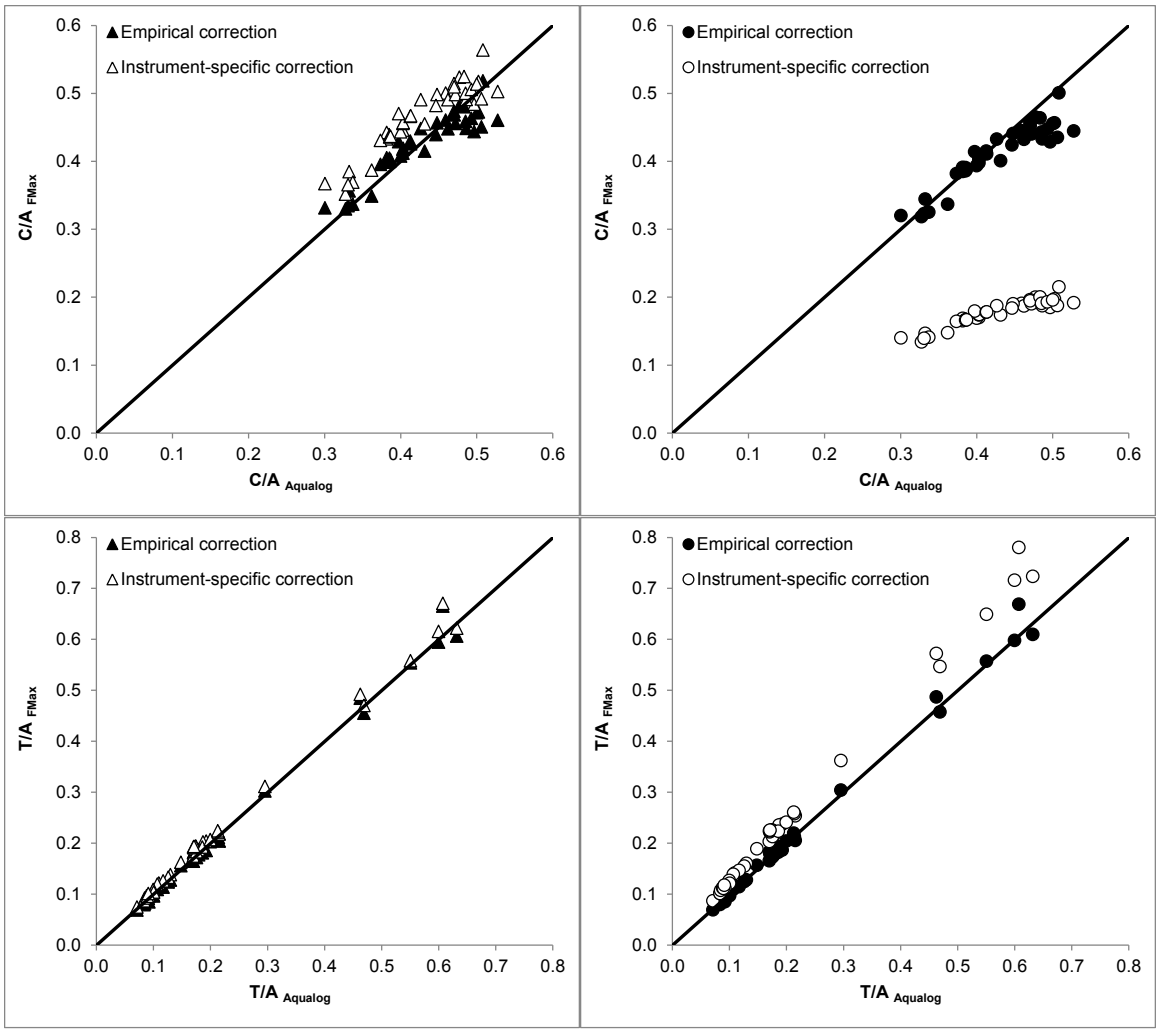

Figure 2.10. The ratio of fluorescence intensity of peaks C to A (C/A) and T to A (T/A) measured on the Fluoromax-4 and Aqualog plotted against each other along with a 1:1 line. Triangles are used for samples where the Fluoromax-4 data was corrected using $excorr_{FM\text{-}rhod}$ and $emcorr_{FM\text{-}OrigHoriba}$. Circles are used for samples where the Fluroomax-4 data corrected using $excorr_{FM\text{-}HoribaKit}$ and $emcorr_{FM\text{-}SRM}$. Open symbols represent samples corrected only with the respective instrument-specific correction factors and shaded symbols represent samples further corrected with an empirically derived inter-instrument correction factor.

APPENDIX

Supporting Information for Chapter One

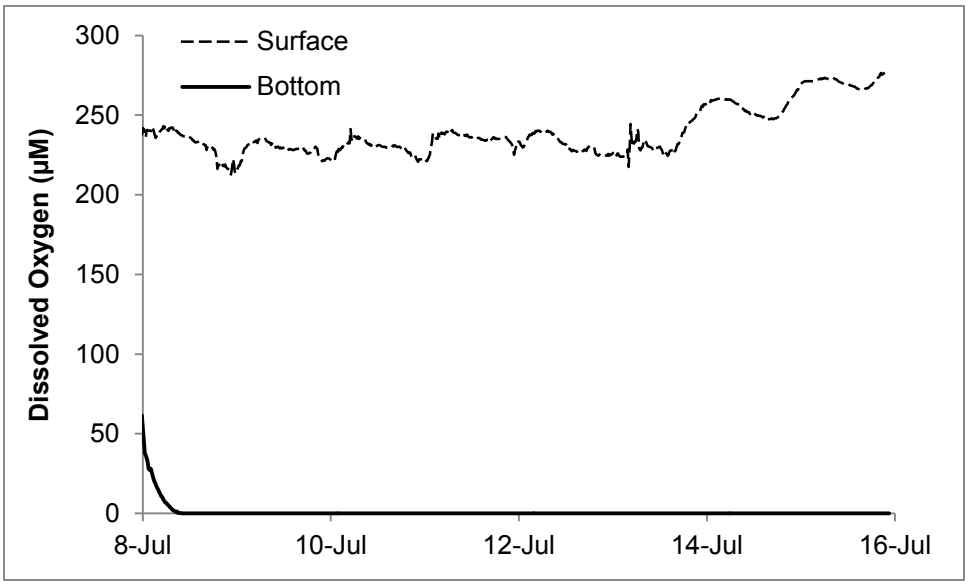

SI Figure 1. During an intensive monitoring of pool 2 under stratified conditions, the surface water (dashed line) exhibited diel fluctuations in dissolved oxygen concentrations but was always well oxygenated (percent saturation ranged from 73 to 95 %). The bottom water (solid line) was anoxic during the entire period except for a brief period of stabilization follow the probe installation.

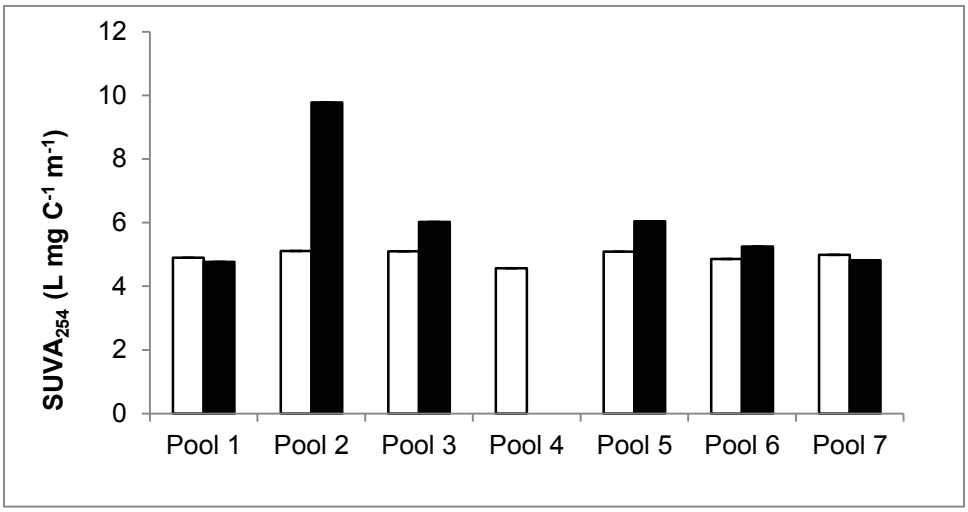

SI Figure 2. Specific UV absorbance at 254 nm ($SUVA_{254}$) values of surface (open bars) and bottom (shaded bars) waters on 14 July, 2011 (error bars of average replicate instrumental analytical error are smaller than can be resolved). Stratified pools almost always had higher $SUVA_{254}$ in the bottom waters than the surface waters. There was no significant difference in $SUVA_{254}$ in pool 1, which mixed daily. Stratified pool 7 also had no significant difference between the surface and bottom.

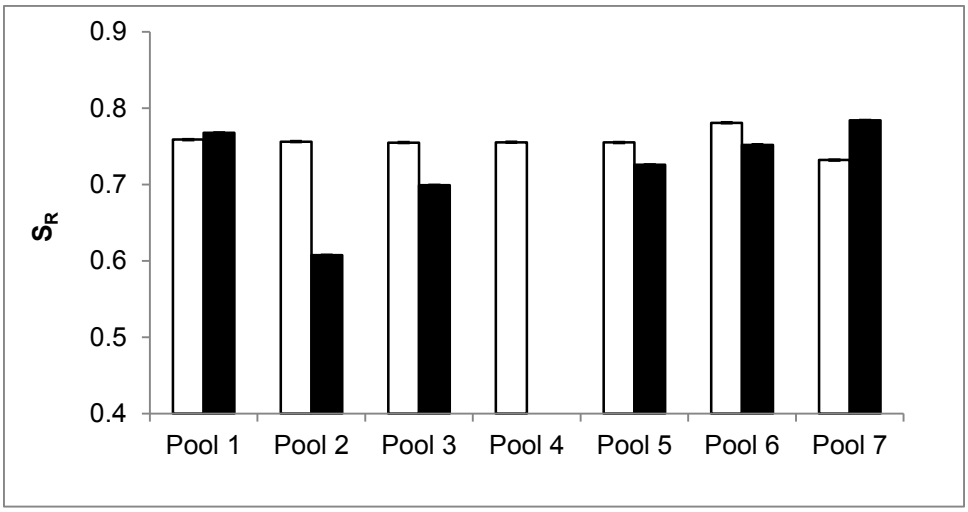

SI Figure 3. Slope ratio (S_R) values of surface (open bars) and bottom (shaded bars) waters on 14 July, 2011 (error bars of average replicate instrumental analytical error are smaller than can be resolved). Stratified pools almost always had higher S_R in the surface waters than the bottom waters. There was no significant difference in S_R in pool 1, which mixed daily. Stratified pool 7 showed lower S_R in the surface compared to bottom, which is the only pool sampled on any date that showed lower S_R in the surface compared to the bottom.

REFERENCES

Albrecht-Gray, A.-M. and Crumbliss, A. L.: Coordination chemistry of siderophores: thermodynamics and kinetics of iron chelation and release, in Iron Transport and Storage in Microorganisms, Plants, and Animals, vol. 35, edited by A. Sigel and H. Sigel, pp. 239–316, CRC Press., 1998.

Battin, T. J., Kaplan, L. A., Findlay, S., Hopkinson, C. S., Marti, E., Packman, A. I., Newbold, J. D. and Sabater, F.: Biophysical controls on organic carbon fluxes in fluvial networks, Nature Geoscience, 2(8), 595–595, doi:10.1038/ngeo602, 2009.

Bencala, K. E. and Walters, R. A.: Simulation of solute transport in a mountain pool-and-riffle stream: A transient storage model, Water Resources Research, 19(3), 718–724, 1983.

Biddanda, B. A. and Cotner, J. B.: Enhancement of Dissolved Organic Matter Bioavailability by Sunlight and Its Role in the Carbon Cycle of Lakes Superior and Michigan, Journal of Great Lakes Research, 29(2), 228–241, doi:10.1016/S0380-1330(03)70429-8, 2003.

Brinkmann, T., Sartorius, D. and Frimmel, F. H.: Photobleaching of humic rich dissolved organic matter, Aquatic Sciences - Research Across Boundaries, 65(4), 415–424, doi:10.1007/s00027-003-0670-9, 2003.

Brooks, P. D. and Williams, M. W.: Snowpack controls on nitrogen cycling and export in seasonally snow-covered catchments, Hydrological Processes, 13, 2177–2190, 1999.

Cauwet, G.: DOM in the coastal zone, in Biogeochemistry of marine dissolved organic matter, edited by D. A. Hansell and C. A. Carlson, pp. 579–611, Academic Press, Boston., 2002.

Coble, P. G., Green, S. A., Blough, N. V. and Gagosian, R. B.: Characterization of dissolved organic matter in the Black Sea by fluorescence spectroscopy, Nature, 348(6300), 432–435, doi:10.1038/348432a0, 1990.

Coble, P. G., Schultz, C. a. and Mopper, K.: Fluorescence contouring analysis of DOC intercalibration experiment samples: a comparison of techniques, Marine Chemistry, 41(1-3), 173–178, doi:10.1016/0304-4203(93)90116-6, 1993.

Cole, J. J., Prairie, Y. T., Caraco, N. F., McDowell, W. H., Tranvik, L. J., Striegl, R. G., Duarte, C. M., Kortelainen, P., Downing, J. a., Middelburg, J. J. and Melack, J.: Plumbing the Global Carbon Cycle: Integrating Inland Waters into the Terrestrial Carbon Budget, Ecosystems, 10(1), 172–185, doi:10.1007/s10021-006-9013-8, 2007.

Cory, R. M., Crump, B. C., Dobkowski, J. A. and Kling, G. W.: Surface exposure to sunlight stimulates CO2 release from permafrost soil carbon in the Arctic, Proceedings of the National Academy of Sciences, 1–6, doi:10.1073/pnas.1214104110, 2013.

Cory, R. M. and Kaplan, L. A.: Biological lability of streamwater fluorescent dissolved organic matter, Limnology and Oceanography, 57(5), 1347–1360, doi:10.4319/lo.2012.57.5.1347, 2012.

Cory, R. M., McKnight, D. M., Chin, Y.-P., Miller, P. L. and Jaros, C. L.: Chemical characteristics of fulvic acids from Arctic surface waters: Microbial contributions and photochemical transformations, Journal of Geophysical Research, 112(G4), 1–14, doi:10.1029/2006JG000343, 2007.

Cory, R. M., Miller, M. P., McKnight, D. M., Guerard, J. J. and Miller, P. L.: Effect of instrument-specific response on the analysis of fulvic acid fluorescence spectra, Limnology and Oceanography: Methods, 8, 67–78, doi:10.4319/lom.2010.8.67 67, 2010.

DeRose, P. C., Early, E. A. and Kramer, G. W.: Qualification of a fluorescence spectrometer for measuring true fluorescence spectra., The Review of scientific instruments, 78(3), 033107, doi:10.1063/1.2715952, 2007.

Detterman, R. L., Bowsher, A. L. and Dutro Jr., J. T.: Glaciation on the Arctic Slope of the Brooks Range, Northern Alaska, Arctic, 11(1), 43–61, 1958.

Fee, E. J., Hecky, R. E., Kasian, S. E. M. and Cruikshank, D. R.: Effects of lake size, water clarity, and climatic variability on mixing depths in Canadian Shield lakes, Limnology and Oceanography, 41(5), 912–920, 1996.

Gao, H. and Zepp, R. G.: Factors Influencing Photoreactions of Dissolved Organic Matter in a Coastal River of the Southeastern United States, Environmental Science & Technology, 32(19), 2940–2946, doi:10.1021/es9803660, 1998.

Gareis, J. A. L., Lesack, L. F. W. and Bothwell, M. L.: Attenuation of in situ UV radiation in Mackenzie Delta lakes with varying dissolved organic matter compositions, Water Resources Research, 46(9), n/a–n/a, doi:10.1029/2009WR008747, 2010.

Goodwin, J. and Whitten, C.: Chelation of ferrous sulphate solutions by desferrioxamine B, Nature, 205(4968), 281–283, 1965.

Hamilton, T. D.: Late Cenozoic glaciation of the central Brooks Range, in Glaciation in Alaska: the geologic record, edited by T. D. Hamilton, K. M. Reed, and R. M. Thorson, pp. 9–50, Alaska Geological Society., 1986.

Hammerschmidt, C. R. and Fitzgerald, W. F.: Iron-mediated photochemical decomposition of methylmercury in an arctic Alaskan lake., Environmental Science & Technology, 44(16), 6138–43, doi:10.1021/es1006934, 2010.

Helms, J. R., Stubbins, A., Ritchie, J. D., Minor, E. C., Kieber, D. J. and Mopper, K.: Absorption spectral slopes and slope ratios as indicators of molecular weight, source, and photobleaching of chromophoric dissolved organic matter, Limnology and Oceanography, 53(3), 955–969, doi:10.4319/lo.2008.53.3.0955, 2008.

Hinzman, L. D., Kane, D. L., Gieck, R. E. and Everett, K. R.: Hydrologic and thermal properties of the active layer in the Alaskan Arctic, Cold Regions Science and Technology, 19, 95–110, 1991.

Holbrook, R. D., DeRose, P. C. and Leigh, S. D.: Excitation-emission matrix fluorescence spectroscopy for natural organic matter characterization: A quantitative evaluation of calibration and spectral correction procedures, Applied Spectroscopy, 60(7), 791–799, doi:10.1366/000370206777886973, 2006.

Kane, D. L., Gieck, R. E., Kitover, D. C., Hinzman, L. D., McNamara, J. P. and Yang, D.: Hydrological cycle on the North Slope of Alaska, in Northern Research Basins Water Balance, edited by D. L. Kane and D. Yang, pp. 224–236, IAHS Press, Wallingford., 2004.

Kane, D. L. and Hinzman, L. D.: Climate data from the North Slope Hydrology Research project, , accessed Feb. 2013, 2011.

Kane, D. L., Hinzman, L. D., Benson, C. S. and Everett, K. R.: Hydrology of Imnavait Creek , an Arctic watershed, Holarctic Ecology, 12(3), 262–269, 1989.

Kane, D. L., Hinzman, L. D., McNamara, J. P., Zhang, Z. and Benson, C. S.: An Overview of a Nested Watershed Study in Arctic Alaska, Nordic Hydrology, 4/5(31), 245–266, 2000.

Kling, G. W., Kipphut, G. W. and Miller, M. C.: Lakes and Streams for Tundra Carbon Budgets Atmosphere : Implications, Science, 251(4991), 298–301, 1991.

Kögel-Knabner, I., Hatcher, P. G. and Zech, W.: Chemical structural studies of forest soil humic acids: aromatic carbon fraction, Soil Science Society of America …, 55(1), 241–247, 1991.

Lakowicz, J. R.: Principles of fluorescence spectroscopy, 3rd ed., Springer., 2006.

Lipson, D. A., Jha, M., Raab, T. K. and Oechel, W. C.: Reduction of iron (III) and humic substances plays a major role in anaerobic respiration in an Arctic peat soil, Journal of Geophysical Research, 115(June), 1–13, doi:10.1029/2009JG001147, 2010.

Lipson, D. A., Zona, D., Raab, T. K., Bozzolo, F., Mauritz, M. and Oechel, W. C.: Water-table height and microtopography control biogeochemical cycling in an Arctic coastal tundra ecosystem, Biogeosciences, 9(1), 577–591, doi:10.5194/bg-9-577-2012, 2012.

Luther III, G. W., Kostka, J. E., Church, T. M., Sulzberger, B. and Stumm, W.: Seasonal iron cycling in the salt-marsh sedimentary environment: the importance of ligand complexes with Fe(II) and Fe(III) in the dissolution of Fe(III) minerals and pyrite, respectively, Marine Chemistry, 40(1-2), 81–103, doi:10.1016/0304-4203(92)90049-G, 1992.

Maranger, R. and Pullin, M. J.: Elemental Complexation by Dissolved Organic Matter in Lakes: Implications for Fe Speciation and the Bioavailability of Fe and P, in Aquatic Ecosystems: Interactivity of Dissolved Organic Matter, pp. 185–214., 2002.

McGlynn, B. ., McDonnell, J. ., Shanley, J. . and Kendall, C.: Riparian zone flowpath dynamics during snowmelt in a small headwater catchment, Journal of Hydrology, 222(1-4), 75–92, doi:10.1016/S0022-1694(99)00102-X, 1999.

McGuire, A. D., Anderson, L. G., Christensen, T. R., Dallimore, S., Guo, L., Hayes, D. J., Heimann, M., Lorenson, T. D., Macdonald, R. W. and Roulet, N.: Sensitivity of the carbon cycle in the Arctic to climate change, Ecological Monographs, 79(4), 523–555, 2009.

McGuire, K. J., Weiler, M. and McDonnell, J. J.: Integrating tracer experiments with modeling to assess runoff processes and water transit times, Advances in Water Resources, 30(4), 824–837, doi:10.1016/j.advwatres.2006.07.004, 2007.

McKnight, D. M., Boyer, E. W., Westerhoff, P. K., Doran, P. T., Kulbe, T. and Andersen, D. T.: Spectrofluorometric characterization of dissolved organic matter for indication of precursor organic material and aromaticity, Limnology and Oceanography, 46(1), 38–48, doi:10.4319/lo.2001.46.1.0038, 2001.

McNamara, J. P., Kane, D. L. and Hinzman, L. D.: An analysis of streamflow hydrology in the Kuparuk River Basin, Arctic Alaska: a nested watershed approach, Journal of Hydrology, 206(1-2), 39–57, doi:10.1016/S0022-1694(98)00083-3, 1998.

McNamara, J. P., Kane, D. L., Hobbie, J. E. and Kling, G. W.: Hydrologic and biogeochemical controls on the spatial and temporal patterns of nitrogen and phosphorus in the Kuparuk River, arctic Alaska, Hydrological Processes, 22, 3294–3309, doi:10.1002/hyp.6902, 2008.

Merck, M. F. and Neilson, B. T.: Modelling in-pool temperature variability in a beaded arctic stream, Hydrological Processes, 26(25), 3921–3933, doi:10.1002/hyp.8419, 2012.

Merck, M. F., Neilson, B. T., Cory, R. M. and Kling, G. W.: Variability of in-stream and riparian storage in a beaded arctic stream, Hydrological Processes, doi:10.1002/hyp.8323, 2011.

Miller, D. C., Kempe, M. D., Kennedy, C. E. and Kurtz, S. R.: Analysis of Transmitted Optical Spectrum Enabling Accelerated Testing of CPV Designs., 2009a.

Miller, M. P., McKnight, D. M., Chapra, S. C. and Williams, M. W.: A model of degradation and production of three pools of dissolved organic matter in an alpine lake, Limnology and Oceanography, 54(6), 2213–2227, doi:10.4319/lo.2009.54.6.2213, 2009b.

Miller, M. P., Simone, B. E., McKnight, D. M., Cory, R. M., Williams, M. W. and Boyer, E. W.: New light on a dark subject: comment, Aquatic Sciences, 72(3), 269–275, doi:10.1007/s00027-010-0130-2, 2010.

Morrice, J. A., Valett, H. M., Dahm, C. N. and Campana, M. E.: Alluvial characteristics, groundwater-surface water exchange and hydrological retention in headwater streams, Hydrological Processes, 11, 253–267, 1997.

Morris, D. P., Zagarese, H., Williamson, C. E., Balseiro, E. G., Hargreaves, B. R., Modenutti, B., Moeller, R. and Queimalinos, C.: The attenuation of solar UV radiation in lakes and the role of dissolved organic carbon, Limnology and Oceanography, 40(8), 1381–1391, 1995.

Mulholland, P. J., Wilson, G. V. and Jardine, P. M.: Hydrogeochemical Response of a Forested Watershed to Storms: Effects of Preferential Flow Along Shallow and Deep Pathways, Water Resources Research, 26(12), 3021–3036, doi:10.1029/WR026i012p03021, 1990.

Neilands, J. B.: Microbial iron compounds, Annual Review of Biochemistry, 50, 715–731, 1981.

Neilson, B. T., Hatch, C. E., Ban, H. and Tyler, S. W.: Solar radiative heating of fiber-optic cables used to monitor temperatures in water, Water Resources Research, 46(8), W08540, doi:10.1029/2009WR008354, 2010.

Osterkamp, T. E. and Payne, M. W.: Estimates of Permafrost Thickness From Well Logs in Northern Alaska, Cold Regions Science and Technology, 5, 13–27, 1981.

Ping, C.-L., Michaelson, G. J., Jorgenson, M. T., Kimble, J. M., Epstein, H., Romanovsky, V. E. and Walker, D. a.: High stocks of soil organic carbon in the North American Arctic region, Nature Geoscience, 1(9), 615–619, doi:10.1038/ngeo284, 2008.

Pullin, M. J., Anthony, C. and Maurice, P. A.: Effects of Iron on the Molecular Weight Distribution, Light Absorption, and Fluorescence Properties of Natural Organic Matter, Environmental Engineering Science, 24(8), 987–997, doi:10.1089/ees.2006.0040, 2007.

Pullin, M. J. and Cabaniss, S. E.: The effects of pH, ionic strength, and iron–fulvic acid interactions on the kinetics of non-photochemical iron transformations. I. Iron(II) oxidation and iron(III) colloid formation, Geochimica et Cosmochimica Acta, 67(21), 4067–4077, doi:10.1016/S0016-7037(03)00366-1, 2003a.

Pullin, M. J. and Cabaniss, S. E.: The effects of pH, ionic strength, and iron–fulvic acid interactions on the kinetics of non-photochemical iron transformations. II. The kinetics of thermal reduction, Geochimica et Cosmochimica Acta, 67(21), 4079–4089, doi:10.1016/S0016-7037(03)00367-3, 2003b.

Pullin, M. J., Progess, C. and Maurice, P. A.: Effects of photoirradiation on the adsorption of dissolved organic matter to goethite, Geochimica et Cosmochimica Acta, 68(18), 3643–3656, doi:10.1016/j.gca.2004.03.017, 2004.

SanClements, M. D., Oelsner, G. P., McKnight, D. M., Stoddard, J. L. and Nelson, S. J.: New insights into the source of decadal increases of dissolved organic matter in acid-sensitive lakes of the northeastern United States., Environmental science & technology, 46(6), 3212–9, doi:10.1021/es204321x, 2012.

Sarmiento, J. L. and Sundquist, E. T.: Revised budget for the oceanic uptake of anthropogenic carbon dioxide, Nature, 356, 589–593, 1992.

Schlesinger, W. H. and Melack, J. M.: Transport of organic carbon in the world's rivers, Tellus, 33(2), 172–187, doi:10.1111/j.2153-3490.1981.tb01742.x, 1981.

Schuur, E. A. G., Bockheim, J. G., Canadell, J. G., Euskirchen, E., Field, C. B., Goryachkin, S. V., Hagemann, S., Kuhry, P., Lafleur, P. M., Lee, H. and others: Vulnerability of permafrost carbon to climate change: Implications for the global carbon cycle, BioScience, 58(8), 701–714, 2008.

Serreze, M. C. and Francis, J. a.: The Arctic Amplification Debate, Climatic Change, 76(3-4), 241–264, doi:10.1007/s10584-005-9017-y, 2006.

Southworth, B. A. and Voelker, B. M.: Hydroxyl radical production via the photo-Fenton reaction in the presence of fulvic acid., Environmental Science & Technology, 37(6), 1130–6, 2003.

Stedmon, C. A. and Bro, R.: Characterizing dissolved organic matter fluorescence with parallel factor analysis: a tutorial, Limnology and Oceanography: Methods, 1–6, 2008.

Stedmon, C. A. and Markager, S.: Optics of chromophoric dissolved organic matter (CDOM) in the Greenland Sea: An algorithm for differentiation between marine and terrestrially derived organic matter, Limnology and Oceanography, 46(8), 2087–2093, 2001.

Stieglitz, M., Shaman, J., McNamara, J., Engel, V., Shanley, J. and Kling, G. W.: An approach to understanding hydrologic connectivity on the hillslope and the implications for nutrient transport, Global Biogeochemical Cycles, 17(4), n/a–n/a, doi:10.1029/2003GB002041, 2003.

Stookey, L. L.: Ferrozine - a new spectrophotometric reagent for iron, Analytical Chemistry, 42(7), 779–781, doi:10.1021/ac60289a016, 1970.

Stumm, W. and Lee, G. F.: Oxygenation of Ferrous Iron, Industrial and Engineering Chemistry, 53(2), 143–146, 1961.

Tarnocai, C., Canadell, J. G., Schuur, E. A. G., Kuhry, P., Mazhitova, G. and Zimov, S.: Soil organic carbon pools in the northern circumpolar permafrost region, Global Biogeochemical Cycles, 23(2), 1–11, doi:10.1029/2008GB003327, 2009.

Walker, D. A., Binnian, E., Evans, B. M., Lederer, N. D., Nordstrand, E. and Webber, P. J.: Terrain, vegetation and landscape evolution of the R4D research site, Brooks Range Foothills, Alaska, Holarctic Ecology, 12(3), 238–261, 1989.

Weishaar, J. L., Aiken, G. R., Bergamaschi, B. A., Fram, M. S., Fujii, R. and Mopper, K.: Evaluation of specific ultraviolet absorbance as an indicator of the chemical composition and reactivity of dissolved organic carbon., Environmental science & technology, 37(20), 4702–8, 2003.

White, E. M., Vaughan, P. P. and Zepp, R. G.: Role of the photo-Fenton reaction in the production of hydroxyl radicals and photobleaching of colored dissolved organic matter in a coastal river of the southeastern United States, Aquatic Sciences - Research Across Boundaries, 65(4), 402–414, doi:10.1007/s00027-003-0675-4, 2003.

Witter, A. E., Hutchins, D. A., Butler, A. and Luther III, G. W.: Determination of conditional stability constants and kinetic constants for strong model Fe-binding ligands in seawater, Marine Chemistry, 69, 1–17, 2000.

Xie, H., Zafiriou, O. C., Cai, W.-J., Zepp, R. G. and Wang, Y.: Photooxidation and its effects on the carboxyl content of dissolved organic matter in two coastal rivers in the southeastern United States., Environmental Science & Technology, 38(15), 4113–9, 2004.